Title

The balance between antiviral and antibacterial responses during *M. tuberculosis* infection is regulated by the ubiquitin ligase CBL

Authors:

Tina Truong1,2, Kelsey Martin1, Michelle Salemi3, Abigail Ray1,4, Brett S. Phinney3, Bennett H. Penn*1,5

Affiliations:

1. Department of Internal Medicine, University of California, Davis, Davis, California, United States of America

2. Graduate Group in Immunology, University of California, Davis, Davis, California, United States of America

3. Proteomics Core Facility, University of California, Davis, Davis, California, United States of America

4. Microbiology Graduate Group, University of California, Davis, Davis, California, United States of America

5. Department of Medical Microbiology and Immunology, University of California, Davis, Davis, California, United States of America

*Corresponding author

Email: bhpenn@ucdavis.edu

Abstract

As a first line of host defense, macrophages must be able to effectively sense and respond to diverse types of pathogens, and while a particular type of immune response may be beneficial in some circumstances, it can be detrimental in others. Upon infecting a macrophage, *M. tuberculosis* (*Mtb*) induces proinflammatory cytokines that activate antibacterial responses. Surprisingly, *Mtb* also triggers antiviral responses that actually hinder the ability of macrophages to control *Mtb* infection. The ubiquitin ligase CBL suppresses these antiviral responses and shifts macrophages toward a more antibacterial state during *Mtb* infection, however, the mechanisms by which CBL regulates immune signaling are unknown. We found that CBL controls responses to multiple stimuli and broadly suppresses the expression of antiviral effector genes. We then used mass-spectrometry to investigate potential CBL substrates and identified over 46,000 ubiquitylated peptides in *Mtb*-infected macrophages, as well as roughly 400 peptides with CBL-dependent ubiquitylation. We then performed genetic interaction analysis of CBL and its putative substrates, and identified the Fas associated factor 2 (FAF2) adapter protein as a key signaling molecule protein downstream of CBL. Together, these analyses identify thousands of new ubiquitin-mediated signaling events during the innate immune response and reveal an important new regulatory hub in this response.

Introduction

Being among the first cells to respond to infection, tissue macrophages must be able to sense and effectively respond to diverse types of pathogens, ranging from multicellular eukaryotic parasites to bacteria and viruses. Longstanding clinical observations have suggested potential antagonism between immune responses targeting different classes of microbes. Patients with preceding influenza virus infection carry roughly a 100-fold higher near-term risk of developing bacterial pneumonia from *Streptococcus pneumoniae* (1). Similarly, while CD4 T helper 2 (Th2)

47 cells are critical for responses to multicellular parasites, patients with Th2-dominant immune
48 responses in *Mycobacterium leprae* lesions harbor higher bacterial loads and experience more
49 severe disease (2).

50 Even in the simple scenario of a single immune cell encountering a lone pathogen, the
51 mechanisms by which the type of pathogen is discerned, and an appropriate response mounted
52 remains poorly understood. Dozens of individual sensors for diverse bacterial-, fungal-, and virus-
53 associated PAMPS have been described (3,4). However, many pathogens, including *M.*
54 *tuberculosis* (*Mtb*), activate multiple sensors simultaneously. How macrophages integrate
55 multiple, sometimes discordant, pathogen-associated signals into a coherent, pathogen-
56 appropriate, response remains unclear.

57 *Mtb* persists as a threat to human health. It currently infects one-third of the world's
58 population, causing a chronic, often lifelong infection, and tuberculosis (TB) kills an estimated 1-
59 2 million people annually (5). Macrophages infected with *Mtb* are immediately exposed to an array
60 of cell wall-derived pathogen-associated molecular patterns (PAMPs) such as lipoproteins,
61 peptidoglycan and trehalose 6,6'-dimycolate, which activate cognate receptors such as TLR2,
62 NOD2 and CLEC4E (Mincle) (6–14). The outcome of many of these signaling pathways is the
63 activation of nuclear factor kappa B (NFκB) family transcription factors and the upregulation of
64 proinflammatory cytokines such as TNF and IL1B which activate potent antibacterial responses
65 and are critical for controlling *Mtb* replication (15–22).

66 Surprisingly, *Mtb* also activates numerous antiviral effectors in infected macrophages. *Mtb*
67 rapidly permeabilizes its phagosome and releases bacterial nucleic acids into the host cytosol
68 through unclear mechanisms (24–26). Bacterial DNA is recognized by cyclic GMP-AMP synthase
69 (cGAS) which then triggers a cascading activation of STING1, TBK1 and the transcription factors
70 IRF3 and IRF7. These induce hundreds of genes, including the type I interferons like interferon
71 beta (IFN-β) that propagate the signal to nearby cells (24–31). Bacterial RNA is also introduced

72 into the host cell, initiating signaling through the retinoic acid-Inducible gene I (RIG-I) sensor which
73 triggers MAVS-dependent activation of IRF3/IRF7 with similar effects (25). While these initial
74 observations came from mouse models, gene expression analysis of TB patients has detected
75 similar activation of type I IFN in the peripheral blood of patients with active TB (32–34).

76 Several lines of evidence demonstrate that these antiviral responses interfere with the
77 antibacterial capacity of macrophages, and suggest that macrophages can be polarized into
78 antiviral or antibacterial states by their encounter with a pathogen. C3H-derived strains of mice
79 harbor a polymorphism causing loss of the SP140 transcriptional repressor, resulting in
80 hyperactivation IFN-β. These strains are highly susceptible to *Mtb*, succumbing rapidly with
81 dramatically increased bacterial burdens (35–39) – a phenotype that is rescued by the
82 administration of an IFN-β blocking antibody or by loss of the type I interferon receptor (IFNAR)
83 (39,40). C57BL/6 mice infected with *Mtb* produce lower levels of IFN-β following infection, but
84 even in this context, loss of MAVS or IFNAR results in decreased bacterial burden and increased
85 survival of infected animals (25,26) Thus, activation of antiviral responses within the host seems
86 to actively interfere with an effective antibacterial response to *Mtb*, and suggests that *Mtb* might
87 introduce nucleic acids into the host cell as a virulence strategy,

88 Ubiquitin signaling plays an important role in regulating both antibacterial and antiviral
89 responses in *Mtb*-infected macrophages. Ubiquitin ligases such as PARKIN and SMURF are
90 critical in targeting *Mtb* for autophagy (41–44). Separately, the ubiquitin ligases TRIM14 and CBL
91 have been shown to regulate the expression of type I interferon following *Mtb* infection (45,46).
92 CBL is targeted by the secreted *Mtb* virulence factor LpqN, which is required for *Mtb* replication
93 in mice (45). Proteomic analyses identified a physical interaction between LpqN and CBL, and
94 the growth of the attenuated *lpqN Mtb* mutant was rescued by disruption of host *Cbl*. While *Cbl*-
95 deficient macrophages are more permissive for *Mtb* replication, the opposite is seen with viral
96 challenge, as CBL-deficient macrophages more potently restrict viral replication (45). Together,

these findings suggest that CBL is an important regulator of the balance between antiviral versus antibacterial responses in macrophages. However, how CBL regulates this process is not known.

Here, we investigated the mechanisms by which CBL regulates immune signaling. We found that it controls macrophage responses to multiple stimuli and represses the expression of numerous antiviral effectors. We then used proteomics to identify potential CBL substrates in macrophages as they respond to *Mtb* infection and identified the endoplasmic reticulum-localized signaling adapter Fas-associated factor 2 (FAF2) as a protein that undergoes CBL-dependent ubiquitylation. Notably, while CBL deficient macrophages are more permissive for *Mtb* growth, simultaneous loss of FAF2 in double-knockout macrophages reverses this phenotype, suggesting that the FAF2 pathway might be hijacked by *Mtb,* and that CBL acts to constrain FAF2 activity in *Mtb*-infected macrophages.

Results

CBL broadly suppresses antiviral effector expression.

Prior work has shown that CBL suppressed host antiviral responses in mouse primary bone-marrow-derived macrophages (BMDMs) following *Mtb* infection (45). We began by assessing whether this role of CBL was evolutionarily conserved, with CBL also regulating these processes in human cells. We used shRNA to deplete CBL mRNA in the human THP-1 cell line that differentiates into macrophage-like cells after stimulation with phorbol-12-myristate-13-acetate (PMA) and 1,25-dihydroxy-vitamin D, and found an ~85% reduction in CBL mRNA levels (Fig 1A). We first assessed whether loss of CBL in human macrophages would similarly rescue the growth of the CBL-sensitive *lpqN* mutant *Mtb* strain which lacks the effector that normally antagonizes CBL function, and which is attenuated in both mouse BMDMs and in mice (45). Following differentiation, we infected THP-1 control cells expressing a non-targeting shRNA, and CBL-depleted cells expressing a CBL-specific shRNA. To monitor bacterial replication, we used

121 the *lpqN Mtb* mutant carrying a *LuxBCADE* bioluminescent reporter operon (45), and monitored
122 bacterial growth over time by quantifying luminescence. Consistent with prior observations in
123 mouse BMDMs, we found that loss of CBL also rescued the growth of the *lpqN* mutant in human
124 macrophages (Fig 1B). The increased bacterial replication was confirmed by direct colony forming
125 unit (CFU) numeration (Fig S1A) and was associated with a more rapid loss of macrophage
126 viability in CBL-deficient macrophages over the course of infection (Fig 1C). The effect of CBL on
127 *Mtb* replication was independently verified using a second independent shRNA in THP-1 cells (Fig
128 S1B). To confirm these findings, we also evaluated the role of CBL in a second human
129 macrophage line, HL-60. Using shRNA to deplete CBL in these cells (Fig 1D) we found that loss
130 of CBL similarly rescued the growth of the *lpqN* mutant in HL-60 cells as well (Fig 1E).

131 **Fig 1. CBL suppresses antiviral responses in human cells.** (A) CBL expression analyzed by
132 RT-qPCR analysis of THP-1 cells expressing CBL-specific shRNA or a control non-targeting
133 shRNA. (B) Luminescent growth assay of CBL-sensitive *lpqN Mtb* mutant carrying the *LuxBCADE*
134 operon. (C) Phase-contrast microscopy images of the same monolayer of THP-1 macrophages
135 prior to infection and 96 h post-infection by *lpqN Mtb* (MOI=0.8, 10x magnification; scale bar
136 100μm). (D) RT-qPCR analysis of CBL expression in HL-60 cells. (E) Luminescent growth assay
137 of *lpqN Mtb* in HL-60 cells. (F),(G) RT-qPCR analysis of *lpqN Mtb*-infected macrophages 6 h after
138 infection. Analysis of (H) THP-1 or (I) HL60 cells transfected with either RNA or DNA as indicated.
139 Error bars denote SEM of technical replicates; statistical significance was evaluated by two-tailed
140 t-test and indicated on plot: *$p \leq 0.05$, **$p \leq 0.01$, ***$p \leq 0.001$, ns $p > 0.05$. Representative (median)
141 data of three or more independent experiments are shown.

142 We next determined whether expression of antiviral effectors was also regulated by CBL
143 in human cells. Consistent with prior observations in mouse macrophages, we found that
144 depletion of CBL resulted in an increased expression of antiviral effectors in both THP-1 and HL-
145 60 cells following *Mtb* infection (Fig 1F,G). We next used defined PAMPs to selectively stimulate

146 different pathways leading to IFN-β activation to assess if CBL was regulating a single sensor
147 pathway or multiple pathways. Work from several groups has shown that *Mtb* activates IFN-β both
148 through the cGAS DNA sensing pathway as well as the RIG-I RNA sensing pathway (24-25,31-
149 32). To assess which pathways are regulated by CBL, we individually transfected THP-1 and HL-
150 60 macrophages with either dsDNA, a known agonist for cGAS, or with 5′-phosphorylated RNA,
151 a known agonist for RIG-I, in order to evaluate the role of CBL. We found that in response to either
152 DNA or 5' phosphorylated RNA, loss of CBL resulted in an increased expression of IFN-β in THP-
153 1 cells (Fig 1H). In HL-60 cells we observed a similar role for CBL in regulating RNA-stimulated
154 IFN-β responses. However, following DNA stimulation HL-60 cells displayed only weak induction
155 of IFN-β, and did so independently of CBL (Fig 1I). Taken together these data support a model
156 where the role of CBL in innate immunity is evolutionarily conserved, acting to suppress
157 expression of antiviral effectors such as IFN-β in multiple different contexts.

158 We next sought to determine whether CBL selectively regulated a restricted group of
159 genes, such as IFIT1 and IFN-β, or whether it orchestrated broad transcriptional changes in
160 macrophages as they responded to *Mtb*. To assess this, we infected THP-1 cells with *Mtb*, using
161 the *lpqN* mutant strain so that CBL activity would be unconstrained by the bacterial effector. We
162 infected both control and CBL-deficient THP-1 cells for 6 h, a time at which many immune-related
163 genes are strongly induced, and prepared RNA for expression profiling by RNA-Seq. As expected,
164 *Mtb* infection of control cells triggered widespread gene expression changes with upregulation of
165 735 genes and downregulation of 423 genes (FDR≤0.05, Log2 fold-change>0.5) and strong
166 induction of both proinflammatory and antiviral effectors. (Fig S2A, Table S1). CBL-deficient cells
167 regulated most of these genes in a similar manner following *Mtb* infection. However, a set of genes
168 showed distinct CBL-dependent transcriptional changes, with 204 genes hyperactivated and 62
169 genes depressed in CBL-deficient cells following *Mtb* infection (Fig 2A and Table S1). Interestingly,
170 while CBL regulates the production of IFN-β in these cells (Fig 1G,I) it does not regulate their

171 response to IFN-β stimulation (Fig S2B), suggesting that the broad CBL-dependent gene
172 expression changes are due to cell-intrinsic mechanisms rather than the indirect effects of type I
173 interferon.

174 **Fig 2. CBL regulates a complex transcriptional program.** (A) RNA-Seq gene expression
175 analysis of THP-1 macrophages expressing CBL-specific shRNA vs control non-targeting shRNA
176 6 h after infection with *lqpN*-mutant *Mtb*. (B) Biological processes transcriptionally regulated by
177 CBL. (C), (D) Differential expression of immunity-related genes in CBL-deficient cells. (E)
178 ENCODE Transcription factor binding site enrichment of CBL-regulated genes (F) RT-qPCR
179 analysis of CBL-regulated genes after indicated stimuli. Differentially-expressed genes for
180 analyses in (B-E) defined by RNA-Seq FDR<0.05 and Log2 fold-change>0.5. RNA-Seq analysis
181 was performed on 3 independent experiments. For RT-qPCR, error bars denote SEM of technical
182 replicates; statistical significance assessed with two-tailed t-test and indicated on plot.
183 Representative (median) data of three independent experiments are shown.

184 We further analyzed the set of genes regulated by CBL to evaluate which cellular
185 processes were being affected, and what transcription factors might be mediating the regulatory
186 effects of CBL. We performed systematic pathway enrichment analysis using the Gene Ontology
187 and KEGG Databases and identified several clusters of functionally-related genes regulated by
188 CBL. Supporting the hypothesis that CBL broadly suppresses antiviral responses, we found a
189 significant over-representation of antiviral defense genes in the set of CBL-regulated genes (10-
190 fold over-representation, FDR <0.02). We also found significant associations with several other
191 pathways including IL-10 production and global protein translation (Fig 2B-D). In addition, we
192 analyzed the set of genes transcriptionally regulated by CBL to determine whether any
193 associations existed between these genes and characterized transcriptional regulators. We
194 assessed this by systematically querying the ENCODE Chip-Seq database (47) with the set of
195 genes regulated by CBL. In uninfected cells, there were no transcriptional regulators enriched at

196 these genes. In contrast, in *Mtb*-infected cells, analysis of the 266 CBL-responsive genes using
197 ENCODE showed an association with several transcriptional regulators (Fig 2E). The most
198 significant association was seen with for the NFkB family member RELA, with an odds-ratio (OR)
199 of 2.6 ($p \leq 1E-9$) found at a set of immune-related genes, with additional associations noted for
200 STAT2 (OR=5.3, $p \leq 2E-7$), ATF1 (OR=2.5, $p \leq 1.1E-8$), and MYC (OR=2.1, $p \leq 5E-8$), suggesting
201 that these transcription factors might be mediating the transcriptional effects of CBL.

202 We also assessed whether genes we identified as regulated by CBL during *Mtb* infection
203 were also regulated by CBL in response to other stimuli. We selected TLR8 and CXCL10, two
204 genes identified by our RNA-Seq analysis of *Mtb*-infected macrophages whose expression was
205 suppressed by CBL, and examined their regulation in cells exposed other PAMPs - either
206 cytoplasmic dsDNA to activate cGAS or 5'-phosphorylated RNA to activate RIG-I. In both cases
207 we found hyperactivation of these genes in CBL-deficient cells, although the patterns differed
208 somewhat. For TLR8 we detected basal de-repression in unstimulated cells and hyperactivation
209 following Mtb infection and either DNA or RNA stimulation. For CXCL10, there was no basal de-
210 repression, and while CXCL10 was strongly regulated by CBL during *Mtb* infection, it showed only
211 modest increases in expression in CBL-deficient cells stimulated with DNA or RNA (Fig 2F). Taken
212 together, these results demonstrate that CBL regulates a broad subset of antiviral response genes
213 in macrophages, along with regulation of several other processes, and that it does so in response
214 to multiple stimuli.

215 **CBL enzymatic activity is required to regulate macrophage responses to Mtb**

216 We next sought to determine the mechanisms by which CBL regulates immune responses.
217 CBL is a RING-domain E3 ligase that was initially characterized as a proto-oncogene,
218 ubiquitylating activated receptor tyrosine kinases to target them for degradation (48–50).
219 Subsequent studies using an enzymatically inactive CBL point mutant showed that CBL also has
220 important non-enzymatic functions, and can act as a signaling scaffold that potentiates

221 phosphatidylinositol 3-kinase and SRC-family kinase activity (51). This non-enzymatic function
222 plays an important role in vivo, as several of the developmental defects *Cbl*$^{-/-}$ mice could be
223 rescued by expression of enzymatically-inactive CBL (52).

224 To test whether CBL was acting enzymatically to ubiquitylate key substrates during innate
225 immune responses, or whether it was acting as a signaling adapter protein, we performed genetic
226 complementation analysis in CBL-deficient macrophages, re-introducing either wild type CBL or
227 catalytically inactive mutants (Fig 3A). To study human macrophages, we used shRNA-expressing
228 CBL-deficient THP-1 cells. To study mouse macrophages we used Cas9-expressing conditionally-
229 immortalized macrophages (CIMs) which are mouse myeloid precursor cells that carry a HOXB8-
230 ER estrogen-regulatable transcription factor. This maintains the cells as immortalized precursors
231 in the presence of estrogen, but upon estrogen withdrawal allows differentiation into macrophages
232 closely recapitulating the physiology of primary mouse BMDMs (53). These cells display high-
233 efficiency genome editing, and transduction of CIM cells with a CBL-specific sgRNA led to a >95%
234 reduction in CBL protein levels in the population (Fig 3B).

235 For both mouse and human cells, we used lentiviral vectors to deliver either catalytically
236 inactive CBL (human C381A, mouse C379A) or WT CBL. In both cases, CBL expression was
237 restored to ~50% of endogenous levels, without evidence of destabilization of the mutant protein
238 (Fig 3B). As seen previously (45), CBL-deficient macrophages were more permissive for *Mtb*
239 replication than control cells, and as expected, in both mouse and human macrophages, re-
240 introduction of WT CBL significantly restricted the growth of *Mtb* (Fig 3C,D). In contrast, re-
241 introduction of catalytically-inactive CBL failed to complement the defective host response,
242 demonstrating that enzymatic activity is needed for CBL function in this context. Interestingly cells
243 expressing inactive CBL actually had higher bacterial loads than CBL-deficient cells, suggesting
244 that catalytically-inactive CBL might act as a dominant-negative isoform, perhaps by interfering
245 with the activity of other signaling molecules such as the related CBL-family ligase CBLB.

246 **Fig 3. CBL-dependent ubiquitylation is required to restrict *Mtb* growth in mouse and human**
247 **macrophages.** (A) CBL domain structure and catalytic site mutants. (B) Immunoblot of wild-type
248 and mutant CBL isoforms expressed from lentiviral vectors in CBL-deficient human (THP-1) and
249 mouse (CIM) macrophages. (C), (D) Luminescent growth assay of *lpqN Mtb* in CBL-deficient
250 macrophages in which CBL expression was restored with either wild-type or mutant CBL. (E)
251 Experimental design for ubiquitylation proteomics using di-Gly MS. (F) di-Gly-MS analysis of
252 ubiquitylation in control CIM cells expressing a non-targeting sgRNA 6 h post-infection with the
253 *lpqN Mtb* mutant. Green (increased) and blue (decreased) indicate peptides with p-value ≤0.01
254 and Log2 fold-change >2. (G) Comparison of ubiquitylation versus total-protein changes in control
255 cells following infection. Green (increased) and blue (decreased) denote data points where the
256 change in di-Gly peptide abundance was >3 standard-deviations greater than the change in
257 protein abundance. (H) Subset of CBL-dependent changes (I) di-Gly MS analysis of ubiquitylation
258 6 h post-infection in control vs. *Cbl*$^{-/-}$ cells infected with *lpqN Mtb*. (J) Ubiquitylation versus total-
259 protein changes in control vs. *Cbl*$^{-/-}$ cells infected with *lpqN Mtb.* (K) Biological process of proteins
260 with CBL-dependent ubiquitylation. MOI=0.8 for growth assays ,and MOI=10 for di-Gly-MS. Di-
261 gly MS was used to analyze 3 independent experiments. For growth assays, representative
262 (median) data of three or more independent experiments are shown; p-value determined by two-
263 tailed t-test and error bars represent SEM of technical replicates.

264 **Identifying potential CBL substrates**

265 Given that the enzymatic activity of CBL was necessary to regulate immune signaling, we
266 next sought to identify CBL substrates in this context. Several growth factor receptors including
267 EGFR, MET, and CSF1R have been characterized as CBL substrates in other settings (48–50).
268 However, the CBL substrates during innate immune responses are not known. We used *Cbl*$^{-/-}$ CIM
269 cells to study ubiquitylation because of the near-complete loss of CBL protein in the polyclonal
270 population of cells expressing a CBL-specific sgRNA, and their larger *Mtb* growth phenotype

271 relative to human cells partially depleted of CBL via shRNA (Fig 3B-D). Using the *lpqN* mutant
272 strain that is unable to antagonize CBL activity, we infected cells for 6 h, and added the
273 proteasome inhibitor bortezomib for the final 2 h to stabilize ubiquitylated proteins and facilitate
274 their detection.

275 We then used di-Gly enrichment and quantitative mass-spectrometry (di-Gly MS) to
276 globally monitor changes in ubiquitylation in *Mtb*-infected cells (Fig 3E). Lysates were prepared
277 from uninfected and infected cells, and from control and *Cbl*$^{-/-}$ cells, and digested with trypsin. We
278 then enriched ubiquitylated peptides by immunoprecipitation with an antibody that recognizes the
279 di-Gly remnant of ubiquitin that remains conjugated to the ubiquitin-modified Lys residue following
280 trypsinization, and analyzed the samples by liquid chromatography tandem MS (LC-MS/MS),
281 using label-free quantification of MS2 spectra (54–59). Of note, the ubiquitin-like proteins ISG15
282 and NEDD8 leave an indistinguishable di-Gly Lys remnant. However, these modifications account
283 for only ~5% of identified di-Gly modified residues, and the vast majority of di-Gly sites are
284 ubiquitin-modified (60–62). In addition, since CBL is a ubiquitin-specific ligase, any CBL-
285 dependent di-Gly modifications should represent CBL-dependent ubiquitylation. Thus, we will
286 hereafter refer to di-Gly-modified sites as ubiquitylation, recognizing that a small percentage of
287 sites modified ligases other than CBL are modified by ISG15 or NEDD8.

288 Overall, we identified ~76,000 unique peptides in macrophages, encompassing ~46,000
289 unique di-Gly-modified sites. This dataset creates the most detailed atlas of ubiquitin modification
290 in macrophages to date, with roughly 10-fold more sites identified than currently available
291 datasets of this specialized cell type. As expected, in control cells, we saw numerous ubiquitin
292 changes in response to *Mtb* with a total of 1,793 ubiquitylation sites increasing (Log2 fold-change
293 >1, FDR <0.05) and 197 sites decreasing (Fig 3F, Table S2). Since the quantity of a ubiquitylated
294 peptide in a sample can change because of either a change in the stoichiometry of ubiquitylation
295 at a given site, or because of a change in abundance of the protein itself, we sought to

296 deconvolute these processes. We examined changes in protein abundance in the same samples
297 by quantitative LC-MS/MS (Table S3) and analyzed the change in ubiquitylation at each site
298 relative to the change in protein expression. This analysis demonstrated a range of stoichiometry
299 changes. For some proteins, such as RSAD2 and IL1B, the increased quantity of ubiquitylated
300 peptides was largely due to increased protein expression (Fig 3G). Conversely, proteins like
301 IKBKE and GABARAP had large changes in ubiquitylation stoichiometry with minimal change in
302 overall protein levels. Overall, changes in abundance of a ubiquitylated peptide and protein
303 abundance were poorly correlated (R^2=0.36) with changes in peptide abundance being driven by
304 changes in stoichiometry of ubiquitylation in roughly 70% of cases.

305 We next examined ubiquitylation in CBL-deficient macrophages following *Mtb* infection.
306 As expected, the loss of CBL did not change the abundance of most ubiquitylated peptides,
307 consistent with a complex ubiquitin signaling landscape involving numerous E3 ligases. However,
308 there was also a clear subset of peptides that underwent CBL-dependent ubiquitylation, including
309 well-established CBL substrates such as the receptor tyrosine kinases MET and CSFR1. As
310 anticipated, most changes seen in *Cbl*$^{-/-}$ cells were peptides with decreased ubiquitylation; there
311 were 430 ubiquitylation sites that decreased (Log2FC >1.0, FDR<0.05) and 90 sites increased in
312 abundance (Fig 3H,I). Changes in the stoichiometry of ubiquitylation drove the changes in
313 abundance of most ubiquitylated peptides, with very little correlation between changes in
314 abundance for ubiquitylated peptides and protein expression (R^2=0.09, Fig 3J).

315 Systematic analysis of the proteins with CBL-dependent ubiquitylation demonstrated the
316 enrichment of several pathways and processes; some had clear immune-related functions such
317 as regulation of phagocytosis (7.1-fold over-representation, p≤0.01), vacuolar acidification (13.7-
318 fold, p=0.02), NFkB regulation (7.2-fold, p=0.02), and IFNGR signaling (4.2-fold, p≤0.01, Fig 3K).
319 There were also factors known to be involved in the immune response to *Legionella pneumophila*
320 (5.3-fold, p≤0.01), *Salmonella enterica* (3.2-fold, p ≤0.001, and *Mtb* itself (3.1-fold, p<0.01).

321 Several other unanticipated pathways were also over-represented in the set of proteins with CBL-
322 dependent ubiquitylation, including endoplasmic reticulum-associated protein degradation
323 (ERAD) pathway (6.2-fold-fold over-representation, p≤0.001) and iron uptake (6.1-fold, p≤0.001).
324 Taken together, these findings suggest that the set of proteins ubiquitylated by CBL extends far
325 beyond its established role in growth-factor signaling at the plasma membrane and includes
326 several other cellular processes throughout the cytoplasm and on membrane-bound organelles.

327 **Function of proteins with CBL-dependent ubiquitylation**

328 We next sought to identify which proteins with CBL-dependent ubiquitylation played
329 important roles during *Mtb* infection. We identified a subset of 43 proteins that had peptides with
330 at least 80% reduction in ubiquitylation in *Cbl*$^{-/-}$ cells. Of these, 20 had annotated functions
331 associated in some way with innate immunity (Fig 4A), and we analyzed this set of 20 proteins
332 for CBL-dependent functions during *Mtb* infection. We hypothesized that if a protein is an
333 important substrate of CBL, then loss of that protein should either phenocopy the CBL mutant (if
334 positively regulated by CBL) or reverse the CBL phenotype (if inhibited by CBL). To analyze each
335 of these factors we designed a lentiviral vector with two sgRNA cassettes, thereby allowing us to
336 generate mutant CIM cell lines lacking either CBL or a putative CBL substrate, as well as double-
337 mutant cells lacking both simultaneously (Fig 4B). Editing efficiency of >80% was confirmed by
338 either TIDE analysis of genomic DNA (85), or by immunoblot of the targeted protein (Fig 4C).

339 **Fig 4. FAF2 promotes *Mtb* replication in the absence of CBL.** (A) Examples of changes in
340 ubiquitylation and total protein for immune regulators in *Mtb*-infected *Cbl*$^{-/-}$ CIM cells 6 h post-
341 infection. In the case of proteins with multiple ubiquitylated peptides, the peptide with greatest
342 statistically-significant fold-change is shown. (B) Experimental design for creation of cells lacking
343 both *Cbl* and putative substrates. (C) Immunoblot of FAF2 protein in CIM cells expressing either
344 non-targeting or *Faf2*-specific sgRNA. (D) Luminescent growth assay of CBL-sensitive *lpqN Mtb*.
345 (E) Location of ubiquitylated residues on FAF2 and Log2 fold-change of ubiquitylation at each

residue site in *Mtb*-infected *Cbl*$^{-/-}$ cells vs. control cells. (F) Immunoblot of FAF2 protein levels in *Mtb*-infected control and *Cbl*$^{-/-}$ cells. Error bars denote SEM of technical replicates; statistical significance was evaluated by two-tailed t-test. Representative (median) data of 4 independent experiments is shown.

We then infected each of these mutant cell lines with the CBL-sensitive *lpqN Mtb* mutant and assessed bacterial growth. As expected, the growth of *Mtb* was more rapid in CBL-deficient cells (Fig 4D), and in most cases, loss of a putative substrate in these CBL-deficient cells did not alter the replication of *Mtb* (data not shown). However, disruption of the Fas-associated factor 2 (*Faf2*) locus in CBL-deficient cells significantly altered the antibacterial capacity of these cells toward *Mtb*. FAF2 is an ER-localized signaling adapter protein, and our di-Gly MS analysis found it to be heavily ubiquitylated in macrophages, with 9 different ubiquitylated Lys residues. In *Cbl*$^{-/-}$ cells, a single residue (K246) showed a specific loss of ubiquitylation, with other Lys residues relatively unaffected (Fig 4E). In contrast to the other genes tested, disruption of FAF2 in CBL-deficient cells restored the ability of these cells to restrict *Mtb* replication, with bacterial growth rates approaching that seen in control macrophages that received a non-targeting sgRNA (Fig 4D).

Given the established role of CBL in targeting growth factor receptors for degradation, we tested the idea that CBL similarly targets FAF2 for degradation through ubiquitylation. However, FAF2 protein levels did not change following Mtb infection and were unaltered in CBL-deficient macrophages (Fig 4F). This suggests that rather than regulating FAF2 levels, CBL-dependent ubiquitylation is instead regulating the function of FAF2, perhaps by altering its protein-protein interactions. Taken together, these genetic analyses show that multiple proteins undergo CBL-dependent ubiquitylation, and FAF2 seems to be an important regulatory hub downstream of CBL as macrophages respond to *Mtb* infection.

Discussion

371 **Antiviral versus antibacterial polarization**

372 Macrophages must be able to sense and effectively respond to diverse types of
373 pathogens. Both clinical data and animal models indicate that while a particular type of immune
374 response may be beneficial in some circumstances, it can be detrimental in others. Tissue
375 macrophages act as first responders in many infections, acting both to eliminate pathogens and
376 to orchestrate subsequent immune responses. However, how a macrophage determines the type
377 of pathogen it is encountering and translates that into an appropriate response remains unclear.

378 *Mtb* exposes an infected macrophage to an array of PAMPS; some are distinctively
379 bacterially-derived molecules such as peptidoglycan or lipoarabinomannan , which activate NOD2
380 and TLR2 respectively. Activation of these sensors results in the release of cytokines with potent
381 antibacterial activities such as TNF and IL1B (5–8,10,11). However, *Mtb*, as well as a number of
382 other intracellular bacterial pathogens, including *Listeria monocytogenes,* and *Chlamydia*
383 *trachomatis,* also activate cytosolic nucleic-acid sensors such as cGAS and induce expression of
384 type I interferon and other antiviral effectors (63–66). While type I interferon potently inhibits
385 viruses and can inhibit the growth of some bacteria such as *C. trachomatis*, it impairs antibacterial
386 responses to *Mtb* and *L. monocytogenes* in mice (63–66).

387 The observation that antiviral responses can actively antagonize the antibacterial capacity
388 of a macrophage suggests that macrophages might become polarized into antibacterial versus
389 antiviral states. It also suggests that pathogens infecting macrophages like *Mtb,* and *L.*
390 *monocytogenes* might seek to subvert this process as a virulence strategy. In the case of *Mtb*, it
391 seems to do so through several mechanisms. First, upon perforating its phagosome, *Mtb* exposes
392 bacterial dsDNA to the host cell cytoplasm which triggers cGAS-dependent activation of IRF3 and
393 induction of IFN-β, as well as hundreds of other downstream genes, many of which have potent
394 antiviral activity (24–31). Second, in parallel, *Mtb* also releases bacterial RNA into the host
395 cytoplasm, thereby activating a similar RIG-I-dependent activation of IRF3, resulting in IFN-β

396 expression (25). *Mtb* also introduces the LpqN virulence factor into host cells which interferes with
397 the ability of the CBL ubiquitin ligase to regulate this process, thereby amplifying antiviral
398 responses (45).

399 Exactly how the expression of antiviral effectors such as IFN-β antagonizes the
400 antibacterial state of a macrophage is unclear. Integrating the results of different studies that
401 examined different viral response regulators suggests that the transcriptional program controlling
402 the expression of antiviral proteins such as IFN-β is likely to be comprised of several distinct
403 modules, as the perturbation of different regulators causes distinct *Mtb*-related phenotypes. For
404 example, in isolated ex vivo macrophages, disruption of CBL, TRIM14, or IRF7 alters the
405 expression of antiviral effectors and alters the ability of a macrophage to restrict *Mtb* replication
406 (45,46,67). In contrast, perturbation of RIG-I, SP140 or IFNAR has no effect on *Mtb* replication in
407 isolated macrophages but profoundly alters *Mtb* susceptibility in mice (25,39,40,67–70). This
408 suggests that while all these pathways regulate IFN-β signaling, they might differ in their
409 regulation of other target genes, and that these differences drive distinct physiologic states in *Mtb*-
410 infected macrophages. It also suggests that the additional regulatory inputs impinging on an
411 infected macrophage during a complex immune response in vivo create a distinct environment
412 where type I interferon signaling becomes a dominant factor.

413 **FAF2 Function**

414 Although the mechanisms by which CBL regulates growth factor signaling are known in
415 detail, the mechanisms by which it regulates innate immunity are not. CBL was initially
416 characterized as a proto-oncogene that ubiquitylates activated receptor tyrosine kinases, thus
417 targeting them for degradation, and was later found to have non-enzymatic functions in activating
418 phosphatidylinositol 3-kinase and SRC-family kinases (48,49,51,71). We found that the enzymatic
419 activity of CBL was needed for its ability to regulate immune responses during *Mtb* infection and
420 identified the signaling adapter protein FAF2 as a critical intermediary factor, as disruption of FAF2

421 rescued the impaired responses in CBL-deficient cells. This suggests a scenario where the
422 pathway regulated by FAF2 might somehow be hijacked by *Mtb* to impair host defenses, and that
423 CBL normally acts to constrain FAF2 activity in *Mtb*-infected macrophages.

424 FAF2 is known to regulate a diverse set of physiologic processes, and thus the manner
425 by which FAF2 regulates the innate immune response to *Mtb* is uncertain. FAF2 was originally
426 characterized as a member of a family of ubiquitin regulatory X (UBX) domain proteins regulating
427 the endoplasmic-reticulum-associated degradation pathway (ERAD) (72). FAF2 was also
428 subsequently shown to act as a positive regulator of STING1, MTOR, and NFκB (73–75). Which
429 of these pathways is the critical one downstream of FAF2 during *Mtb* infection is an important
430 remaining question. It is also unclear what function the CBL-dependent ubiquitylation of FAF2 at
431 K246 plays. A straightforward explanation would have been that CBL inhibits FAF2 by targeting it
432 for degradation, analogous to the regulation of growth-factor receptors (49,76,77). However, our
433 data demonstrate that this is not the case. Instead, it seems that ubiquitylation alters FAF2
434 functionality, perhaps by modulating its interactions with STING1, MTOR, or NFκB or their
435 regulators. Future genetic experiments analyzing FAF2 alleles with mutations in K246 should
436 provide insight into the function of FAF2 ubiquitylation, as will biochemical experiments analyzing
437 the activation state of these different pathways.

438 **Ubiquitin signaling during *Mtb* infection**

439 These studies also create a detailed map of protein ubiquitylation in macrophages as they
440 respond to a pathogen, generating intriguing new hypotheses about how ubiquitin signaling might
441 regulate innate immunity. Although numerous proteomics studies have analyzed ubiquitylation in
442 mammalian cells, few of these focused on immune cells, and only a handful have examined
443 signaling during innate immune responses to pathogens. Such studies in activated immune cells
444 have provided important insights by identifying specific ubiquitylation events contributing to
445 autophagy and DNA repair processes during infection that alter immune responses (78,79). Here,

446 we identified ~46,000 unique di-Gly-modified Lys residues, an in-depth dataset that significantly
447 broadens the understanding of the ubiquitin-mediated signaling events taking place in
448 macrophages as they respond to a pathogen. These analyses reveal a number of previously
449 unknown ubiquitylation events on critical immune regulators, including the secreted cytokines
450 IL1A and TNFSF13B, the endosomal peptidoglycan transporter SLC15A3, and the cytoplasmic
451 peptidoglycan sensor NOD2 (Table S2). Thus, this dataset suggests multiple new mechanisms
452 by which ubiquitin signaling might be regulating other critical immune responses.

453 **Limitations**

454 While our RNA-Seq data show clear CBL-dependent transcriptional changes in CBL-
455 depleted THP-1 macrophages, this is an imperfect model system. The expression of CBL is only
456 reduced ~85% by shRNA, and it is possible that residual CBL activity could be masking some
457 changes. Although we also used CRISPR/Cas9 genome-editing to generate *CBL*$^{-/-}$ THP-1 clones,
458 we observed marked clone-to-clone variability in *Mtb*-related phenotypes making it an unsuitable
459 alternative. In addition, the response of cell lines such as THP-1 cells to immune stimuli is often
460 muted relative to primary macrophages (53). For example, we note that while changes in IFN-β
461 expression were readily detectible in *Mtb*-infected THP-1 cells by RT-qPCR, the overall transcript
462 levels were too low for reliable quantification by RNA-Seq. Separately, our MS studies had some
463 limitations. They identified a large number of peptides with the di-Gly remnant, and while ~95%
464 of di-Gly Lys modifications result from ubiquitylation, NEDD8 and ISG15 both leave identical di-
465 Gly remnants. Our current data are unable to distinguish the small subset of Lys residues modified
466 by these other ubiquitin-related proteins. However, since CBL is believed to be a ubiquitin-specific
467 ligase the set of CBL-dependent changes are likely due to ubiquitin. Finally, for those proteins
468 with CBL-dependent ubiquitylation, we cannot distinguish at this time between direct ubiquitylation
469 by CBL versus indirect effects mediated by another E3 ligase or deubiquitinase that CBL

470 regulates, an analysis that will require complex in vitro ubiquitylation systems with MS analysis of
471 reaction products, and important future direction.

472

473 **SUPPLEMENTAL FIGURE AND TABLE LEGENDS**

474 **Fig S1.** (A) CFU determination in THP-1 cells expressing either CBL-specific or non-targeting
475 control shRNA 5d after infection with *lpqN Mtb.* (B) Luminescent growth assay of *lpqN Mtb* in THP-
476 1 cells depleted of CBL by a second independent shRNA.

477 **Fig S2.** (A) RNA-seq analysis of control THP-1 cells expressing a non-targeting shRNA,
478 comparing uninfected cells and *lpqN Mtb*-infected cells. (B) RT-qPCR analysis of IFIT1 in IFN-β
479 stimulated THP-1 cells.

480 **Table S1** RNA-Seq Dataset

481 **Table S2** Di-Gly MS Dataset

482 **Table S3** Total Protein MS dataset

483

484 # Materials & Methods

485

486 **Key Reagent Table**

REAGENT OR RESOURCE	SOURCE	IDENTIFIER
Antibodies		
Rabbit c-CBL antibody	Cell Signaling Technology	Cat # 2747
β-Actin (C4) Alexa Fluor® 680	Santa Cruz Biotechnology	Cat # sc-47778 AF680
PTMScan® Ubiquitin Remnant Motif (K-ε-GG)	Cell Signaling Technology	Cat # 5562S
FAF2 antibody	Proteintech	Cat # 16251-1-AP
IRDye® 800CW Donkey anti-Mouse IgG Secondary Antibody	Li-cor	Cat # 926-32212
IRDye® 800CW Goat anti-Rabbit IgG Secondary Antibody	Li-cor	Cat # 926-32211
Primer and guide sequences		
qPCR_*IFNβ* Human F	This paper	CTTCTCCACTACAGCTCTTTCC
qPCR_*IFNβ* Human R	This paper	GCCAGGAGGTTCTCAACAATA

qPCR_*IFIT1* Human F	This paper	CCAGAAATAGACTGTGAGGAAGG
qPCR_*IFIT1* Human R	This paper	CCCTATCTGGTGATGCAGTAAG
qPCR_*β-ACTIN* Human F	This paper	GACCACCTTCAACTCCATCAT
qPCR_*β-ACTIN* Human R	This paper	CCTGCTTGCTAATCCACATCT
ms_*Actin*_qpcr_FW	This paper	GGTGTGATGGTGGGAATGG
ms_*Actin*_qpcr_RV	This paper	GCCCTCGTCACCCACATAGGA
ms_*Ifnβ*_qPCR_FW	This paper	TCCGAGCAGAGATCTTCAGGAA
ms_*Ifnβ*_qPCR_RV	This paper	TGCAACCACCACTCATTCTGAG
ms_*Ifit1*_qPCR_FW	This paper	CGTAGCCTATCGCCAAGATTTA
ms_*Ifit1*_qPCR_RV	This paper	AGCTTTAGGGCAAGGAGAAC
Lg_m*Faf2*gRNA_Rv	This paper	AGTTACGCGTCTCTAAACCCATG
		TTCCAGTTATGCTGCGGGAAAGA
		GTGGTCTCATACAG
Lg_m*Faf2*geno_Fw	This paper	CTAGTAGTTACAGTGTGCTTGC
Lg_m*Faf2*geno_Rv	This paper	CTGTGAACATTTCTGTTGCTCC
T2A_BSF_F	This paper	GAAGTCTGCTAACATGCGGTGAC
		G
		TCGAGGAGAATCCTGGCCCAATG
		GCCAAG
		CCTTTGTCTCAAG

Strep_T2A_R	This paper	GACGTCACCGCATGTTAGCAGACTTCCCCTG CCCTCGCCGGAGCCGGGCCCCTTCT CGAACTGGGGGTGGCTCCAG
Bla_R_	This paper	CTTTGTACAAGAAAGCTGGGTCTAGAT TTAGCCCTCCCACACATAACCAGAGGGC
Bacterial strains		
CDC1551 *lpqN*:Tnhimar1 mutant	BEI Resources	Cat # NR-18454
Cell lines		
THP-1	ATCC	TIB-202
HL-60	ATCC	CCL-240
HoxB8-ER; Rosa26 Cas9 CIM	Gift from Greg Barton, UC Berkeley	N/A
B16	ATCC	CRL-6475
3T3-MCSF	Gift from Russell Vance, UC Berkeley	

Chemicals		
Middlebrook OADC	Thermo Fisher Scientific	Cat # b12351
BD DIFCO™ Middlebrook 7H9	Becton Dickinson (BD)	Cat # 271310
BD DIFCO™ Middlebrook 7H10	Becton Dickinson (BD)	Cat # 262710
PTMScan Lys-C Protease	Cell Signaling Technology	Cat # 39003
Sequencing Grade Modified Trypsin	Promega	Cat # V5111
Bortezomib	Cell Signaling Technology	Cat # 2204S
cOmplete™, Mini, EDTA-free Protease Inhibitor Cocktail	Sigma Aldrich	Cat # 11836170001
Bovine growth serum	Hycolone	SH30541.03
Fetal bovine serum	Corning	5-015-CV
Phorbol 12-myristate 13 acetate (PMA)	Sigma Aldrich	Cat # P8139
1α,25-Dihydroxyvitamin D3 (Vitamin D)	Santa Cruz	Cat # 32222-06-3
SYBR™ Gold Nucleic Acid Gel Stain	Invitrogen	Cat # S11494
Poly(ethylene glycol) 8000	Sigma	Cat # 81268
Lipofectamine 2000	Invitrogen	Cat # 11668030

Consumables		
500mg Sep-Pak C18 columns	Waters	Cat # WAT036790
PureLink™ RNA Mini Kit	Invitrogen	Cat # 12183018A
Maxima H Minus Reverse Transcriptase	Thermo Scientific	Cat # EP0753
0.45 µm Acrodisc Syringe Filters	Pall	Cat # 4614
Recombinant DNA		
lentiGuide Puro	Addgene	Plasmid #52963
pENTR1a	Thermo	A10462
pLenti CMV blast DEST	Addgene	Plasmid #17451
pLenti CMV no selection marker	This paper	
pLKO.1 puro	Addgene	Plasmid #8453
Software and websites		
Prism v9.0	GraphPad	
Rstudio	Posit	
Synthego guide design tool	Synthego	https://design.synthego.com
TIDE analysis		https://tide.nki.nl/

Other	
Odyssey CLx	Li-Cor
Glomax Explorer	Promega
CFX Connect Real-Time System	BIO-RAD
Whole-body exposure chamber 099C	Glas-Col
A4212	

487

488 **Deposited data**

489 At the time of publication raw MS data files will be deposited at MasIVE
490 https://massive.ucsd.edu/ProteoSAFe. RNA-Seq data will be deposited at GEO
491 https://www.ncbi.nlm.nih.gov /geo/info/seq.html. Processed MS and RNA-Seq data will be
492 available as supplementary data files at the time of publication.

493 **Cell Lines**

494 THP-1 human monocytes (ATCC TIB-202) and HL-60 promyeloblast cells (ATCC CCL-240) were
495 purchased from ATCC. THP-1 cells were cultured in RPMI media containing 10% fetal bovine
496 serum (FBS), 10mM HEPES, 1mM sodium pyruvate, 4500 mg/L glucose, and 0.05 mM 2-
497 mercaptoethanol. HL-60 cells are cultured in RPMI containing 10% bovine growth serum (BGS),
498 15% fetal bovine serum (FBS), 1mM sodium pyruvate, 2mM L-glutamine, and 1X MEM non-
499 essential amino acids solution. HOXB8-ER and Cas9-expressing conditionally immortalized
500 macrophages (CIMs) were cultured in RPMI media containing 10% FBS, 10mM HEPES, 1mM
501 sodium pyruvate, 2mM L-glutamine, 1.5ul 2-mercaptoethanol, 2% GM-CSF as conditioned media
502 from B16 cells murine melanoma cells, and 2uM β-estradiol as previously described (53), prior to

503 differentiation. THP-1 and HL-60 cells were differentiated with DMEM supplemented with 10%
504 FBS, 1mM pyruvate, 2mM L-glutamine, 10ng/ml phorbol 12-myristate 13 acetate (PMA), and
505 0.1ng/ml 1,25 dihydroxy-vitamin D. Cells were differentiated for 72 h before experiments. CIM
506 cells were differentiated by washing to removal of β-estradiol and then culture with DMEM
507 supplemented with 10% FBS, 2mM L-glutamine, 1mM sodium pyruvate, 10% MCSF (derived
508 from 3T3 MCSF conditioned media) for 7 days prior to experiments.

509 All cell lines generated using lentiviral vectors followed the same steps of transfection of
510 HEK 293T Lenti-X cells with the transfer vector expressing the gene of interest, alongside the
511 packaging plasmids psPAX2 and the envelope plasmid VSV-G. Viral supernatant is harvested 48
512 hours after transfection and either filtered with a 0.45 µm syringe filter and for CIM cell
513 transduction, concentrated using A PEG-8000 solution (80). For transduction, viral supernatant
514 with Polybrene 8ug/ml is added for 12h to THP-1 and HL-60 cells. CIM cells are transduced
515 through spinfection and spun for 2h at 1000 RPM at 32C and then incubated for 6h before washing
516 and culture in fresh media. Selective antibiotics were as follows: THP-1 and HL-60 cells are
517 selected with 0.5 μg/ml of Puromycin or 4 μg/ml of Blasticidin. CIM cells are selected with 8 μg/ml
518 of Puromycin or 4 μg/ml of Blasticidin.

519 **Bacterial Strains**

520 *Mtb* was cultured in 7H9 (BD) supplemented with 0.5% glycerol, 10% oleic acid-albumin-dextrose-
521 catalase (OADC, Middlebrook), and 0.1% Tween-80 in bottles gently rotated at 40 RPM at 37° C
522 or on 7H10 plates supplemented with 10% OADC, 0.5% glycerol, and 0.1% Tween 80 at 37° C.

523 **Macrophage Infection for RNA harvest:**

524 *Mtb* strains were prepared for inoculation by washing twice in PBS with 10% heat-inactivated
525 horse serum, gently sonicated, and spun at 500 rpm for 5 m to generate a fine bacterial
526 suspension. Bacteria were opsonized in 10% heat-inactivated horse serum and macrophages

527 were infected at an MOI = 10 for 6hr by spinfection at 1200RPM for 10 minutes followed by
528 washing in PBS. After incubation, wells are washed once with 1X PBS and harvested in Trizol for
529 RNA extraction.

530 **Macrophage Infection for Lux assay:**

531 For luminescent growth assays, cells are plated in triplicate in 96 well plates at a density of 8 x
532 10^4 cells/well for THP-1 cells and 1.5 x 10^5 cells/ well for CIM cells. Macrophage cell density at
533 the time of infection was carefully matched between control and experimental cell lines to within
534 <15% variance by plating sets of control wells across a gradient of densities and using SYBR gold
535 to quantify nucleic acid content of plated experimental and control cells. Macrophages are infected
536 at a MO1 = 0.8, and after spinfection plates are incubated for 30 minutes at 37° C. After the
537 incubation, the monolayers were washed with PBS containing 1% heat-inactivated horse serum
538 twice, and bacterial luminescence was measured over time in a GloMax Explorer warmed to 37
539 degrees C. Macrophage growth media was changed every other day. Colony-forming units
540 (CFUs) were quantified by lysing triplicate wells of macrophages in sterile water and plated in
541 serially dilutions on 7H10 agar with supplemented with OADC and 0.1% Tween-80. Plates were
542 incubated at 37° C for 3 weeks prior to CFU enumeration.

543 **Western Blots**

544 Protein in cell lysates was quantified by BCA. 30-50ug of protein lysate was separated by SDS-
545 PAGE and transferred onto nitrocellulose membranes and blocked with LiCor blocking buffer at
546 0.5x for 1h. Primary antibodies were used at varying dilutions and incubated 1.5h at room-
547 temperature or, in the case of anti-CBL antibody, 4° C overnight. Secondary antibodies were used
548 at 1:10,000 dilution for 1h. After probing for indicated antibodies, the membranes were imaged on
549 an Odyssey scanner (Licor).

550 **RNA Purification**

551 Nucleic acid-stimulated macrophages were lysed in PureLink lysis buffer per manufacturer
552 instructions. *Mtb*- infected macrophages were lysed in Trizol. In both cases, lysates were purified
553 with silica spin columns (Purelink) per manufacturer instructions.

554 **Macrophage nucleic acid stimulation and RT-qPCR**

555 Differentiated THP-1 and HL-60 cells are plated at 8 x 10^5/ well in a 12-well plate. Cells are
556 stimulated with 10ng of RNA or 20ng of DNA delivered by Lipofectamine 2000 as per manufacturer
557 instructions and incubated for 6h. After RNA purification, cDNA was generated using 500ng total
558 RNA with Maxima H minus reverse transcriptase and diluted 1:10 before qPCR analysis with the
559 indicated primers and SYBR Green I detection of products.

560 **RNA-seq**

561 Differentiated THP-1 cells were infected at MOI=10 for 6 h with *lpqN Mtb* in three independent
562 experiments on different days. RNA was purified and barcoded 3'Tag-Seq libraries prepared using
563 the QuantSeq FWD kit (Lexogen, Vienna, Austria) for multiplexed sequencing according to the
564 recommendations of the manufacturer by the UC Davis DNA Sequencing core. The fragment size
565 distribution of the libraries was verified via micro-capillary gel electrophoresis on a Bioanalyzer
566 2100 (Agilent, Santa Clara, CA). The libraries were quantified by fluorometry on a Qubit
567 instrument (Life Technologies, Carlsbad, CA), and pooled in equimolar ratios. Twelve libraries
568 were sequenced on one lane of an Aviti sequencer (Element Biosciences, San Diego, CA) with
569 single-end 100 bp reads. The sequencing generated more than 4 million reads per library.
570 Analysis of human data: HTStream was used to remove PhiX, adapter sequences, polyA tails,
571 low quality sequences from end of reads, N bases, and reads less than 50 basepairs. After
572 preprocessing, STAR was used to align reads to GRCh38.p13 human genome. UMI-tools was
573 used to remove PCR duplicates post-alignment. Next, feature Counts was used to count reads
574 whose alignment overlapped with genes using the gencode genome corresponding to the human

575 genome version used. Annotation used was version 41. R was used for limma-voom pipeline on
576 R with multiple testing correction using Benjamini-Hochberg procedure.

577 **Plasmid Construction for short shRNA and sgRNA delivery**

578 shRNA expression plasmids were constructed by digesting pLKO.1 cloning vector with AgeI and
579 EcoRI and annealed oligonucleotides containing the 21 shRNA encoding sequence were inserted,
580 For sgRNA, 20 nucleotide targeting sequences were designed to target regions in the first exon
581 of each locus using the Synthgo design tool. The targeting sequence is then fused by overlap-
582 extension PCR to a second-generation tracRNA (81) and inserted into the HpaI and XhoI sites of
583 pSicoR . The dual-guide sgRNA vector was constructed using a synthesized gene block
584 containing the two guides of interest and an H1 promoter from Integrated DNA technologies (IDT)
585 that were digested with BsmBI v2 on both ends and ligated to BsmBI v2 digested Lentiguide Puro
586 vector (Addgene) with a second-generation tracRNA (81). Evaluation of editing efficiency was
587 performed using TIDE.

588 **CRISPR/Cas9 genome editing.**

589 After lentiviral delivery of sgRNA cells were selected for 1 week with puromycin. The genome
590 editing efficiency of the polyclonal population evaluated by PCR amplification of the targeted exon
591 followed by Sanger sequencing and TIDE analysis. The polyclonal population was used for
592 experiments.

593 **Site-directed mutagenesis**

594 The wildtype and ligase mutant copies of CBL for both THP-1 and CIM cells contain synonymous
595 mutations at the targeting sites of either the RNAi or CAS9 system to prevent degradation. Site-
596 directed mutagenesis was carried out to generate catalytically inactive CBL mutants using
597 pENTR1a plasmids (Addgene). Mutagenesis was validated through Sanger sequencing.
598 Following validation, gateway cloning was used to move the mutated CBL open reading frame

599 from pENTR1a into lentiviral pDEST vectors (Addgene). For THP-1 cells, constructs were cloned
600 into a pLenti CMV Blast vector (Addgene). For CIM cells, constructs were fused by overlap
601 extension PCR directly to a T2A peptide and blasticidin resistance gene and were cloned into
602 pLenti CMV modified to remove other antibiotic resistance genes (82).

603 **di-Gly Enrichment**

604 3×10^7 cells were plated 24h before infection. Cells were infected with *lpqN Mtb* at an MOI
605 = 10 for 6 hours. 2h prior to harvest, the 1μM of Bortezomib is added. For harvest, cells were
606 washed 1X with PBS then scraped in ice-cold methanol+ 0.1 glycine pH 2.5 to precipitate protein,
607 and inactivate proteases and *Mtb.* Cells were scrapped and removed from the BSL3. Chloroform
608 was added to 20% volume to assist precipitation, incubated on ice for 10 min. and samples
609 centrifuged to pellet protein. The pellets were washed once with ice-cold methanol, recentrifuged,
610 and dried. Protein was resolubilized in in 9M Urea 25 mM HEPES pH 8.5,1 mM chloroacetamide
611 (CAM), 0.5x Complete-mini protease inhibitor, and 0.5 mM EDTA with sonication. Proteins were
612 then reduced for 45 min with 5 mM dithiothreitol (DTT) at room temperature and alkylated with
613 20mM CAM for 20 minutes at room temperature and in the dark. BCA assay was performed,
614 samples diluted 1:4 in HEPES pH 8.0 and 2.5 mg of protein digested with Lys-C at enzyme to
615 substrate ratio 1:100 at 37°C for 2h. Subsequently, samples were digested overnight at 37°C with
616 trypsin enzyme to substrate ratio 1ug:100ug. Digestion was stopped with 0.5% TFA and then
617 incubated on ice for 15 min to allow urea to precipitate and samples centrifuged to pellet debris.
618 Peptides were desalted with 500 mg Sep-Pal C18 columns as per manufacturer instructions and
619 lyophilized.

620 2.5mg of lyophilized peptides were resuspended with 0.5x immunoaffinity purification
621 (IAP) buffer (50mM MOPS, pH7.2; 10mM sodium phosphate; 50mM NaCl) and sonicated. 10 ul
622 cross-linked anti-K-ε-GG antibody beads were washed 3x in PBS. Samples were then mixed with
623 10 ul cross-linked anti-K-ε-GG antibody beads and incubated at 4°C for 2h. The peptide-bead

624 mixture was then washed four times with PBS and one time with 0.1x IAP. Peptides were eluted
625 with 100ul 0.15% TFA and analyzed by LC-MS/MS with on-tip clean up prior to MS run.

626 **Mass-Spectrometry**

627 Chromatography was performed on an Evosep 1 using either the 60spd (di-Gly) or 30spd
628 (total protein) method. Each sample was loaded onto a disposable Evotip C18 trap column
629 (Evosep Biosytems, Denmark) as per the manufacturer's instructions. Briefly, Evotips were wetted
630 with 2-propanol, equilibrated with 0.1% formic acid, and then samples were loaded using
631 centrifugal force at 1200g. Evotips were subsequently washed with 0.1% formic acid, and then
632 200 µL of 0.1% formic acid was added to each tip to prevent drying. The tipped samples were
633 subjected to nanoLC on a Evosep One instrument (Evosep Biosystems). Tips were eluted directly
634 onto a PepSep analytical column, dimensions: 150umx10cm C18 column (PepSep, Denmark)
635 with 1.5 µm particle size (100 Å pores) (Bruker Daltronics), and a ZDV spray emitter (Bruker
636 Daltronics). Mobile phases A and B were 100% water with 0.1% formic acid (v/v) and 100%
637 Acetonitrile 0.1% formic acid (v/v), respectively. The standard pre-set method of 30 samples-per-
638 day was used, which is a 44 min minute run or 60 spd which is a 21 min run.

639 Mass Spectrometry – Performed on a hybrid trapped ion mobility spectrometry-quadrupole
640 time of flight mass spectrometer (timsTOF Pro 2 and timsTOF HT, (Bruker Daltonics, Bremen,
641 Germany) with a modified nano-electrospray ion source (CaptiveSpray, Bruker Daltonics). In the
642 experiments described here, the mass spectrometer was operated in diaPASEF mode.
643 Desolvated ions entered the vacuum region through the glass capillary and deflected into the
644 TIMS tunnel which is electrically separated into two parts (dual TIMS). Here, the first region is
645 operated as an ion accumulation trap that primarily stores all ions entering the mass spectrometer,
646 while the second part performs trapped ion mobility analysis.

647 DIA PASEF: The dual TIMS analyzer was operated at a fixed duty cycle close to 100%
648 using equal accumulation and ramp times of 75 ms each. For the 30spd Evosep run, Data-

649 independent analysis (DIA) scheme consisted of one MS scan followed by MSMS scans taken
650 with 6x3= 18 precursor windows at width of 50Th per 6x3= 560 ms cycle, over the mass range
651 8x3= 300-1200 Dalton. The TIMS scans layer the doubly and triply charged peptides over an ion
652 mobility -1/k0- range of 0.707-1.29 V*sec/cm2. The collision energy was ramped linearly as a
653 function of the mobility from 59 eV at 1/K0=1.2 to 20 eV at 1/K0=0.7. For the 60spd Evosep run,
654 Data-independent analysis (DIA) scheme consisted of one MS scan followed by MS/MS scans
655 taken with 5x7= 35 precursor windows at width of 30^{Th} = 763 ms cycle time over the mass range
656 286-1307 Dalton. The TIMS scans layer the doubly and triply charged peptides over an ion
657 mobility -1/k0- range of 0.7-1.3 V*sec/cm2. The collision energy was ramped linearly as a function
658 of the mobility from 59 eV at 1/K0=1.2 to 20 eV at 1/K0=0.

659 **Data Analysis**

660 LCMS files were processed with Spectronaut version 18.4(Biognosys, Zurich,
661 Switzerland) using DirectDIA analysis mode. Mass tolerance/accuracy for precursor and fragment
662 identification was set to default settings. The unreviewed FASTA for Mus Musculus,
663 UP000000589, downloaded from Uniprot and a universal library of common laboratory
664 contaminants (Frankenfield et al, 2022). For di-Gly analysis, a maximum of two missing cleavages
665 were allowed, the required minimum peptide sequence length was 7 amino acids, and the peptide
666 mass was limited to a maximum of 4600 Da. Carbamidomethylation of cysteine residues was set
667 as a fixed modification, and methionine oxidation, acetylation of protein N termini and
668 ubiquitination as variable modifications. A decoy false discovery rate (FDR) at less than 1% for
669 peptide spectrum matches and protein group identifications was used for spectra filtering
670 (Spectronaut default). Decoy database hits, proteins identified as potential contaminants, and
671 proteins identified exclusively by one site modification were excluded from further analysis. For
672 total protein: DIA data was analyzed using Spectronaut 18. using the direct DIA workflow with
673 PTM localization selected. Trypsin/P Specific was set for the enzyme allowing two missed

674 cleavages. Fixed Modifications were set for Carbamidomethyl, and variable modifications were
675 set to Acetyl (Protein N-term), Oxidation, and ubiquitination. For DIA search identification, PSM
676 and Protein Group FDR were set at 0.01%. Mass-spectrometry statistical analysis was performed
677 in Spectronaut® (Biognosys) using t-test with multiple testing correction.

678 **Pathway enrichment analysis**

679 Functional and pathway enrichment analysis for RNA-seq Ubiquitination Proteomics Gene
680 ontology and pathway analysis were carried out on the set of genes with FDR <= 0.5 and LogFC
681 <= 0.5 using the DAVID database (Database for Annotation, Visualization and Integrated
682 Discovery; https://david.ncifcrf.gov/) (84). The significantly enriched biological pathways were
683 identified with FDR <0.05. The pathways were visualized using R.

684 **Statistics**

685 Statistical significance for RT-qPCR data was performed using GraphPad Prism version
686 10 (GraphPad Software, LLC) using two-tailed Student t-test when comparing. Statistical analysis
687 for RNA-sequencing datasets was performed using the limma-voom pipeline on R with multiple
688 testing corrections using Benjamini-Hochberg procedure. Ubiquitination statistical analysis was
689 carried out within Spectronaut® (Biognosys) using the integrated statistical package with
690 randomized imputation of values near the limit of detection if a peptide was undetectable in a
691 particular sample, and performs t-tests with multiple testing correction and FDR calculation.

692 **Acknowledgements**

693 We would like to thank Sebastian Winter and Jeroen Saeij for their input on this
694 manuscript. We would like to thank the DNA Technologies and Bioinformatics cores at UC Davis
695 that assisted with the sequencing and processing of the RNA-seq analysis. Schematic images
696 were prepared with Biorender. BHP was funded by NIH 1R01AI144149.

697

References

1. Shrestha S, Foxman B, Weinberger DM, Steiner C, Viboud C, Rohani P. Identifying the interaction between influenza and pneumococcal pneumonia using incidence data. Sci Transl Med. 2013 Jun 26;5(191):191ra84.

2. Yamamura M, Uyemura K, Deans RJ, Weinberg K, Rea TH, Bloom BR, et al. Defining Protective Responses to Pathogens: Cytokine Profiles in Leprosy Lesions. Science. 1991 Oct 11;254(5029):277–9.

3. Mogensen TH. Pathogen Recognition and Inflammatory Signaling in Innate Immune Defenses. Clin Microbiol Rev. 2009 Apr;22(2):240–73.

4. Li D, Wu M. Pattern recognition receptors in health and diseases. Sig Transduct Target Ther. 2021 Aug 4;6(1):1–24.

5. TB mortality [Internet]. [cited 2024 Apr 17]. Available from: https://www.who.int/teams/global-tuberculosis-programme/tb-reports/global-tuberculosis-report-2023/tb-disease-burden/1-2-tb-mortality

6. Ferwerda G, Girardin SE, Kullberg BJ, Le Bourhis L, de Jong DJ, Langenberg DML, et al. NOD2 and toll-like receptors are nonredundant recognition systems of Mycobacterium tuberculosis. PLoS Pathog. 2005 Nov;1(3):279–85.

7. Bowdish DME, Sakamoto K, Kim MJ, Kroos M, Mukhopadhyay S, Leifer CA, et al. MARCO, TLR2, and CD14 are required for macrophage cytokine responses to mycobacterial trehalose dimycolate and Mycobacterium tuberculosis. PLoS Pathog. 2009 Jun;5(6):e1000474.

718 8. Underhill DM, Ozinsky A, Smith KD, Aderem A. Toll-like receptor-2 mediates mycobacteria-
719 induced proinflammatory signaling in macrophages. Proc Natl Acad Sci U S A. 1999 Dec
720 7;96(25):14459–63.

721 9. Blumenthal A, Kobayashi T, Pierini LM, Banaei N, Ernst JD, Miyake K, et al. RP105 facilitates
722 macrophage activation by Mycobacterium tuberculosis lipoproteins. Cell Host Microbe. 2009
723 Jan 22;5(1):35–46.

724 10. Means TK, Wang S, Lien E, Yoshimura A, Golenbock DT, Fenton MJ. Human toll-like
725 receptors mediate cellular activation by Mycobacterium tuberculosis. J Immunol. 1999 Oct
726 1;163(7):3920–7.

727 11. Bafica A, Scanga CA, Feng CG, Leifer C, Cheever A, Sher A. TLR9 regulates Th1 responses
728 and cooperates with TLR2 in mediating optimal resistance to Mycobacterium tuberculosis. J
729 Exp Med. 2005 Dec 19;202(12):1715–24.

730 12. Dorhoi A, Nouailles G, Jörg S, Hagens K, Heinemann E, Pradl L, et al. Activation of the NLRP3
731 inflammasome by Mycobacterium tuberculosis is uncoupled from susceptibility to active
732 tuberculosis. Eur J Immunol. 2012 Feb;42(2):374–84.

733 13. Mishra BB, Rathinam VAK, Martens GW, Martinot AJ, Kornfeld H, Fitzgerald KA, et al. Nitric
734 oxide controls the immunopathology of tuberculosis by inhibiting NLRP3 inflammasome-
735 dependent processing of IL-1β. Nat Immunol. 2013 Jan;14(1):52–60.

736 14. Ishikawa E, Ishikawa T, Morita YS, Toyonaga K, Yamada H, Takeuchi O, et al. Direct
737 recognition of the mycobacterial glycolipid, trehalose dimycolate, by C-type lectin Mincle. J
738 Exp Med. 2009 Dec 21;206(13):2879–88.

739 15. Bourigault ML, Segueni N, Rose S, Court N, Vacher R, Vasseur V, et al. Relative contribution
740 of IL-1α, IL-1β and TNF to the host response to Mycobacterium tuberculosis and attenuated
741 M. bovis BCG. Immun Inflamm Dis. 2014/11/18 ed. 2013 Oct;1(1):47–62.

742 16. Segueni N, Benmerzoug S, Rose S, Gauthier A, Bourigault ML, Reverchon F, et al. Innate
743 myeloid cell TNFR1 mediates first line defence against primary Mycobacterium tuberculosis
744 infection. Scientific Reports. 2016 Mar 2;6(1):22454.

745 17. Mayer-Barber KD, Barber DL, Shenderov K, White SD, Wilson MS, Cheever A, et al. Cutting
746 Edge: Caspase-1 Independent IL-1β Production Is Critical for Host Resistance to
747 Mycobacterium tuberculosis and Does Not Require TLR Signaling In Vivo. The Journal of
748 Immunology. 2010 Apr 1;184(7):3326–30.

749 18. Pattanaik KP, Ganguli G, Naik SK, Sonawane A. *Mycobacterium tuberculosis* EsxL induces
750 TNF-α secretion through activation of TLR2 dependent MAPK and NF-κB pathways.
751 Molecular Immunology. 2021 Feb 1;130:133–41.

752 19. Mayer-Barber KD, Andrade BB, Oland SD, Amaral EP, Barber DL, Gonzales J, et al. Host-
753 directed therapy of tuberculosis based on interleukin-1 and type I interferon crosstalk. Nature.
754 2014 Jul 3;511(7507):99–103.

755 20. Di Paolo NC, Shafiani S, Day T, Papayannopoulou T, Russell DW, Iwakura Y, et al.
756 Interdependence between Interleukin-1 and Tumor Necrosis Factor Regulates TNF-
757 Dependent Control of Mycobacterium tuberculosis Infection. Immunity. 2015 Dec
758 15;43(6):1125–36.

759 21. Mayer-Barber KD, Barber DL, Shenderov K, White SD, Wilson MS, Cheever A, et al.
760 Caspase-1 independent IL-1beta production is critical for host resistance to mycobacterium

761 tuberculosis and does not require TLR signaling in vivo. J Immunol. 2010 Apr 1;184(7):3326–
762 30.

763 22. Flynn JL, Goldstein MM, Chan J, Triebold KJ, Pfeffer K, Lowenstein CJ, et al. Tumor necrosis
764 factor-α is required in the protective immune response against Mycobacterium tuberculosis in
765 mice. Immunity. 1995;2(6):561–72.

766 23. 1.2 TB mortality [Internet]. [cited 2024 Apr 17]. Available from:
767 https://www.who.int/teams/global-tuberculosis-programme/tb-reports/global-tuberculosis-
768 report-2023/tb-disease-burden/1-2-tb-mortality

769 24. Wassermann R, Gulen MF, Sala C, Perin SG, Lou Y, Rybniker J, et al. Mycobacterium
770 tuberculosis Differentially Activates cGAS- and Inflammasome-Dependent Intracellular
771 Immune Responses through ESX-1. Cell Host & Microbe. 2015 Jun 10;17(6):799–810.

772 25. Cheng Y, Schorey JS. Mycobacterium tuberculosis–induced IFN-β production requires
773 cytosolic DNA and RNA sensing pathways. J Exp Med. 2018 Nov 5;215(11):2919–35.

774 26. Stanley SA, Johndrow JE, Manzanillo P, Cox JS. The Type I IFN Response to Infection with
775 Mycobacterium tuberculosis Requires ESX-1-Mediated Secretion and Contributes to
776 Pathogenesis1. The Journal of Immunology. 2007 Mar 1;178(5):3143–52.

777 27. Creagh EM, O'Neill LAJ. TLRs, NLRs and RLRs: a trinity of pathogen sensors that co-operate
778 in innate immunity. Trends in Immunology. 2006 Aug 1;27(8):352–7.

779 28. Kawai T, Akira S. The roles of TLRs, RLRs and NLRs in pathogen recognition. Int Immunol.
780 2009 Apr;21(4):317–37.

781 29. Chen W, Han C, Xie B, Hu X, Yu Q, Shi L, et al. Induction of Siglec-G by RNA Viruses Inhibits
782 the Innate Immune Response by Promoting RIG-I Degradation. Cell. 2013 Jan
783 31;152(3):467–78.

784 30. Watson RO, Bell SL, MacDuff DA, Kimmey JM, Diner EJ, Olivas J, et al. The Cytosolic Sensor
785 cGAS Detects Mycobacterium tuberculosis DNA to Induce Type I Interferons and Activate
786 Autophagy. Cell Host & Microbe. 2015 Jun 10;17(6):811–9.

787 31. Collins AC, Cai H, Li T, Franco LH, Li XD, Nair VR, et al. Cyclic GMP-AMP Synthase Is an
788 Innate Immune DNA Sensor for Mycobacterium tuberculosis. Cell Host & Microbe. 2015 Jun
789 10;17(6):820–8.

790 32. Berry MPR, Graham CM, McNab FW, Xu Z, Bloch SAA, Oni T, et al. An interferon-inducible
791 neutrophil-driven blood transcriptional signature in human tuberculosis. Nature. 2010
792 Aug;466(7309):973–7.

793 33. Maertzdorf J, Repsilber D, Parida SK, Stanley K, Roberts T, Black G, et al. Human gene
794 expression profiles of susceptibility and resistance in tuberculosis. Genes Immun. 2011
795 Jan;12(1):15–22.

796 34. Maertzdorf J, Ota M, Repsilber D, Mollenkopf HJ, Weiner J, Hill PC, et al. Functional
797 Correlations of Pathogenesis-Driven Gene Expression Signatures in Tuberculosis. PLOS
798 ONE. 2011 Oct 28;6(10):e26938.

799 35. Moreira-Teixeira L, Tabone O, Graham CM, Singhania A, Stavropoulos E, Redford PS, et al.
800 Mouse transcriptome reveals potential signatures of protection and pathogenesis in human
801 tuberculosis. Nat Immunol. 2020 Apr 1;21(4):464–76.

802 36. Moreira-Teixeira L, Stimpson PJ, Stavropoulos E, Hadebe S, Chakravarty P, Ioannou M, et
803 al. Type I IFN exacerbates disease in tuberculosis-susceptible mice by inducing neutrophil-
804 mediated lung inflammation and NETosis. Nat Commun. 2020 Nov 4;11:5566.

805 37. Kramnik I, Dietrich WF, Demant P, Bloom BR. Genetic control of resistance to experimental
806 infection with virulent Mycobacterium tuberculosis. Proceedings of the National Academy of
807 Sciences. 2000 Jul 18;97(15):8560–5.

808 38. Kamath AB, Alt J, Debbabi H, Behar SM. Toll-Like Receptor 4-Defective C3H/HeJ Mice Are
809 Not More Susceptible than Other C3H Substrains to Infection with Mycobacterium
810 tuberculosis. Infect Immun. 2003 Jul;71(7):4112–8.

811 39. Ji DX, Yamashiro LH, Chen KJ, Mukaida N, Kramnik I, Darwin KH, et al. Type I interferon-
812 driven susceptibility to Mycobacterium tuberculosis is mediated by IL-1Ra. Nature
813 microbiology. 2019;4(12):2128–35.

814 40. Ji DX, Witt KC, Kotov DI, Margolis SR, Louie A, Chevée V, et al. Role of the transcriptional
815 regulator SP140 in resistance to bacterial infections via repression of type I interferons.
816 Stallings CL, Rath S, editors. eLife. 2021 Jun 21;10:e67290.

817 41. Franco LH, Nair VR, Scharn CR, Xavier RJ, Torrealba JR, Shiloh MU, et al. The Ubiquitin
818 Ligase Smurf1 Functions in Selective Autophagy of Mycobacterium tuberculosis and Anti-
819 tuberculous Host Defense. Cell Host Microbe. 2017 Sep 13;22(3):421–3.

820 42. Manzanillo PS, Ayres JS, Watson RO, Collins AC, Souza G, Rae CS, et al. The ubiquitin
821 ligase parkin mediates resistance to intracellular pathogens. Nature. 2013 Sep
822 26;501(7468):512–6.

823 43. Watson RO, Manzanillo PS, Cox JS. Extracellular M. tuberculosis DNA targets bacteria for
824 autophagy by activating the host DNA-sensing pathway. Cell. 2012 Aug 17;150(4):803–15.

825 44. Gutierrez MG, Master SS, Singh SB, Taylor GA, Colombo MI, Deretic V. Autophagy Is a
826 Defense Mechanism Inhibiting BCG and Mycobacterium tuberculosis Survival in Infected
827 Macrophages. Cell. 2004 Dec 17;119(6):753–66.

828 45. Penn BH, Netter Z, Johnson JR, Von Dollen J, Jang GM, Johnson T, et al. An Mtb-Human
829 Protein-Protein Interaction Map Identifies a Switch Between Host Anti-Viral and Anti-Bacterial
830 Responses. Mol Cell. 2018 Aug 16;71(4):637-648.e5.

831 46. Hoffpauir CT, Bell SL, West KO, Jing T, Wagner AR, Torres-Odio S, et al. TRIM14 Is a Key
832 Regulator of the Type I IFN Response during Mycobacterium tuberculosis Infection. J
833 Immunol. 2020 Jul 1;205(1):153–67.

834 47. Landt SG, Marinov GK, Kundaje A, Kheradpour P, Pauli F, Batzoglou S, et al. ChIP-seq
835 guidelines and practices of the ENCODE and modENCODE consortia. Genome Res. 2012
836 Sep;22(9):1813–31.

837 48. Andoniou CE, Lill NL, Thien CB, Lupher ML, Ota S, Bowtell DD, et al. The Cbl proto-oncogene
838 product negatively regulates the Src-family tyrosine kinase Fyn by enhancing its degradation.
839 Molecular and Cellular Biology. 2000;20(3):851–67.

840 49. Duan L, Miura Y, Dimri M, Majumder B, Dodge IL, Reddi AL, et al. Cbl-mediated
841 ubiquitinylation is required for lysosomal sorting of epidermal growth factor receptor but is
842 dispensable for endocytosis. Journal of Biological Chemistry. 2003;278(31):28950–60.

843 50. Andoniou CE, Thien CB, Langdon WY. The two major sites of cbl tyrosine phosphorylation in
844 abl-transformed cells select the crkL SH2 domain. Oncogene. 1996 May 2;12(9):1981–9.

845 51. Arron JR, Vologodskaia M, Wong BR, Naramura M, Kim N, Gu H, et al. A positive regulatory
846 role for Cbl family proteins in tumor necrosis factor-related activation-induced cytokine
847 (trance) and CD40L-mediated Akt activation. J Biol Chem. 2001 Aug 10;276(32):30011–7.

848 52. Thien CB, Blystad FD, Zhan Y, Lew AM, Voigt V, Andoniou CE, et al. Loss of c-Cbl RING
849 finger function results in high-intensity TCR signaling and thymic deletion. The EMBO Journal.
850 2005;24(21):3807–19.

851 53. Roberts AW, Popov LM, Mitchell G, Ching KL, Licht DJ, Golovkine G, et al. Cas9+
852 conditionally-immortalized macrophages as a tool for bacterial pathogenesis and beyond.
853 Garrett WS, Kana BD, editors. eLife. 2019 Jun 17;8:e45957.

854 54. Fulzele A, Bennett EJ. Ubiquitin diGLY proteomics as an approach to identify and quantify
855 the ubiquitin-modified proteome. Methods Mol Biol. 2018;1844:363–84.

856 55. Denis NJ, Vasilescu J, Lambert JP, Smith JC, Figeys D. Tryptic digestion of ubiquitin
857 standards reveals an improved strategy for identifying ubiquitinated proteins by mass
858 spectrometry. Proteomics. 2007 Mar;7(6):868–74.

859 56. Kim W, Bennett EJ, Huttlin EL, Guo A, Li J, Possemato A, et al. Systematic and quantitative
860 assessment of the ubiquitin-modified proteome. Mol Cell. 2011 Oct 21;44(2):325–40.

861 57. Wagner SA, Beli P, Weinert BT, Nielsen ML, Cox J, Mann M, et al. A proteome-wide,
862 quantitative survey of in vivo ubiquitylation sites reveals widespread regulatory roles. Mol Cell
863 Proteomics. 2011 Oct;10(10):M111.013284.

864 58. Xu G, Paige JS, Jaffrey SR. Global analysis of lysine ubiquitination by ubiquitin remnant
865 immunoaffinity profiling. Nat Biotechnol. 2010 Aug;28(8):868–73.

866 59. Udeshi ND, Svinkina T, Mertins P, Kuhn E, Mani DR, Qiao JW, et al. Refined preparation and
867 use of anti-diglycine remnant (K-ε-GG) antibody enables routine quantification of 10,000s of
868 ubiquitination sites in single proteomics experiments. Mol Cell Proteomics. 2013
869 Mar;12(3):825–31.

870 60. Lumpkin RJ, Gu H, Zhu Y, Leonard M, Ahmad AS, Clauser KR, et al. Site-specific
871 identification and quantitation of endogenous SUMO modifications under native conditions.
872 Nat Commun. 2017 Oct 27;8:1171.

873 61. Lobato-Gil S, Heidelberger JB, Maghames C, Bailly A, Brunello L, Rodriguez MS, et al.
874 Proteome-wide identification of NEDD8 modification sites reveals distinct proteomes for
875 canonical and atypical NEDDylation. Cell Rep. 2021 Jan 19;34(3):108635.

876 62. Zhang Y, Thery F, Wu NC, Luhmann EK, Dussurget O, Foecke M, et al. The in vivo ISGylome
877 links ISG15 to metabolic pathways and autophagy upon Listeria monocytogenes infection.
878 Nat Commun. 2019 Nov 26;10(1):5383.

879 63. He R, Torres CA, Wang Y, He C, Zhong G. Type-I Interferon Signaling Protects against
880 Chlamydia trachomatis Infection in the Female Lower Genital Tract. Infect Immun. 2023 Jun
881 15;91(6):e0015323.

882 64. Prantner D, Darville T, Nagarajan UM. Stimulator of IFN gene is critical for induction of IFN-
883 beta during Chlamydia muridarum infection. J Immunol. 2010 Mar 1;184(5):2551–60.

884 65. Leber JH, Crimmins GT, Raghavan S, Meyer-Morse NP, Cox JS, Portnoy DA. Distinct TLR-
885 and NLR-Mediated Transcriptional Responses to an Intracellular Pathogen. PLOS
886 Pathogens. 2008 Jan 11;4(1):e6.

887 66. Woodward JJ, Iavarone AT, Portnoy DA. c-di-AMP secreted by intracellular Listeria
888 monocytogenes activates a host type I interferon response. Science. 2010 Jun
889 25;328(5986):1703–5.

890 67. Johnson JR, Parry T, Repasy T, Geiger KM, Verschueren E, Budzik JM, et al. Comparative
891 analysis of macrophage post-translational modifications during intracellular bacterial
892 pathogen infection [Internet]. bioRxiv; 2020 [cited 2024 Apr 25]. p. 2020.05.27.116772.
893 Available from: https://www.biorxiv.org/content/10.1101/2020.05.27.116772v1

894 68. Bullen CK, Singh AK, Krug S, Lun S, Thakur P, Srikrishna G, et al. MDA5 RNA-sensing
895 pathway activation by Mycobacterium tuberculosis promotes innate immune subversion and
896 pathogen survival. JCI Insight. 2023 Oct 23;8(20):e166242.

897 69. Zhang L, Jiang X, Pfau D, Ling Y, Nathan CF. Type I interferon signaling mediates
898 Mycobacterium tuberculosis-induced macrophage death. J Exp Med. 2021 Feb
899 1;218(2):e20200887.

900 70. Kotov DI, Lee OV, Fattinger SA, Langner CA, Guillen JV, Peters JM, et al. Early cellular
901 mechanisms of type I interferon-driven susceptibility to tuberculosis. Cell. 2023 Dec
902 7;186(25):5536-5553.e22.

903 71. Miyake S, Lupher ML, Druker B, Band H. The tyrosine kinase regulator Cbl enhances the
904 ubiquitination and degradation of the platelet-derived growth factor receptor α. Proceedings
905 of the National Academy of Sciences. 1998;95(14):7927–32.

906 72. Christianson JC, Olzmann JA, Shaler TA, Sowa ME, Bennett EJ, Richter CM, et al. Defining
907 human ERAD networks through an integrative mapping strategy. Nat Cell Biol. 2011 Nov
908 27;14(1):93–105.

909 73. Yang L, Wang L, Ketkar H, Ma J, Yang G, Cui S, et al. UBXN3B positively regulates STING-
910 mediated antiviral immune responses. Nat Commun. 2018 Jun 13;9(1):2329.

911 74. Liu F, Tian T, Zhang Z, Xie S, Yang J, Zhu L, et al. Long non-coding RNA SNHG6 couples
912 cholesterol sensing with mTORC1 activation in hepatocellular carcinoma. Nat Metab. 2022
913 Aug;4(8):1022–40.

914 75. Gwon Y, Maxwell BA, Kolaitis RM, Zhang P, Kim HJ, Taylor JP. Ubiquitination of G3BP1
915 mediates stress granule disassembly in a context-specific manner. Science. 2021 Jun
916 25;372(6549):eabf6548.

917 76. Grøvdal LM, Stang E, Sorkin A, Madshus IH. Direct interaction of Cbl with pTyr 1045 of the
918 EGF receptor (EGFR) is required to sort the EGFR to lysosomes for degradation.
919 Experimental cell research. 2004;300(2):388–95.

920 77. Visser Smit GD, Place TL, Cole SL, Clausen KA, Vemuganti S, Zhang G, et al. Cbl Controls
921 EGFR Fate by Regulating Early Endosome Fusion. Science Signaling. 2009 Dec
922 22;2(102):ra86–ra86.

923 78. Budzik JM, Swaney DL, Jimenez-Morales D, Johnson JR, Garelis NE, Repasy T, et al.
924 Dynamic post-translational modification profiling of Mycobacterium tuberculosis-infected
925 primary macrophages. Elife. 2020 Jan 17;9:e51461.

926 79. Johnson JR, Crosby DC, Hultquist JF, Kurland AP, Adhikary P, Li D, et al. Global post-
927 translational modification profiling of HIV-1-infected cells reveals mechanisms of host cellular
928 pathway remodeling. Cell Rep. 2022 Apr 12;39(2):110690.

929 80. Torii S, Oishi W, Zhu Y, Thakali O, Malla B, Yu Z, et al. Comparison of five polyethylene glycol
930 precipitation procedures for the RT-qPCR based recovery of murine hepatitis virus,

931 bacteriophage phi6, and pepper mild mottle virus as a surrogate for SARS-CoV-2 from
932 wastewater. Science of The Total Environment. 2022 Feb 10;807:150722.

933 81. Tzelepis K, Koike-Yusa H, De Braekeleer E, Li Y, Metzakopian E, Dovey OM, et al. A CRISPR
934 Dropout Screen Identifies Genetic Vulnerabilities and Therapeutic Targets in Acute Myeloid
935 Leukemia. Cell Rep. 2016/10/21 ed. 2016 Oct 18;17(4):1193–205.

936 82. Liu Z, Chen O, Wall JBJ, Zheng M, Zhou Y, Wang L, et al. Systematic comparison of 2A
937 peptides for cloning multi-genes in a polycistronic vector. Sci Rep. 2017 May 19;7(1):2193.

938 83. Mohapatra B, Zutshi N, An W, Goetz B, Arya P, Bielecki TA, et al. An essential role of CBL
939 and CBL-B ubiquitin ligases in mammary stem cell maintenance. Development. 2017 Mar
940 15;144(6):1072–86.

941 84. Sherman BT, Hao M, Qiu J, Jiao X, Baseler MW, Lane HC, et al. DAVID: a web server for
942 functional enrichment analysis and functional annotation of gene lists (2021 update). Nucleic
943 Acids Research. 2022 Jul 5;50(W1):W216–21.

944 85. Brinkman EK, Chen T, Amendola M, van Steensel B. Easy quantitative assessment of
945 genome editing by sequence trace decomposition. Nucleic Acids Res. 2014 Dec
946 16;42(22):e168.

947

948

FIGURE 1

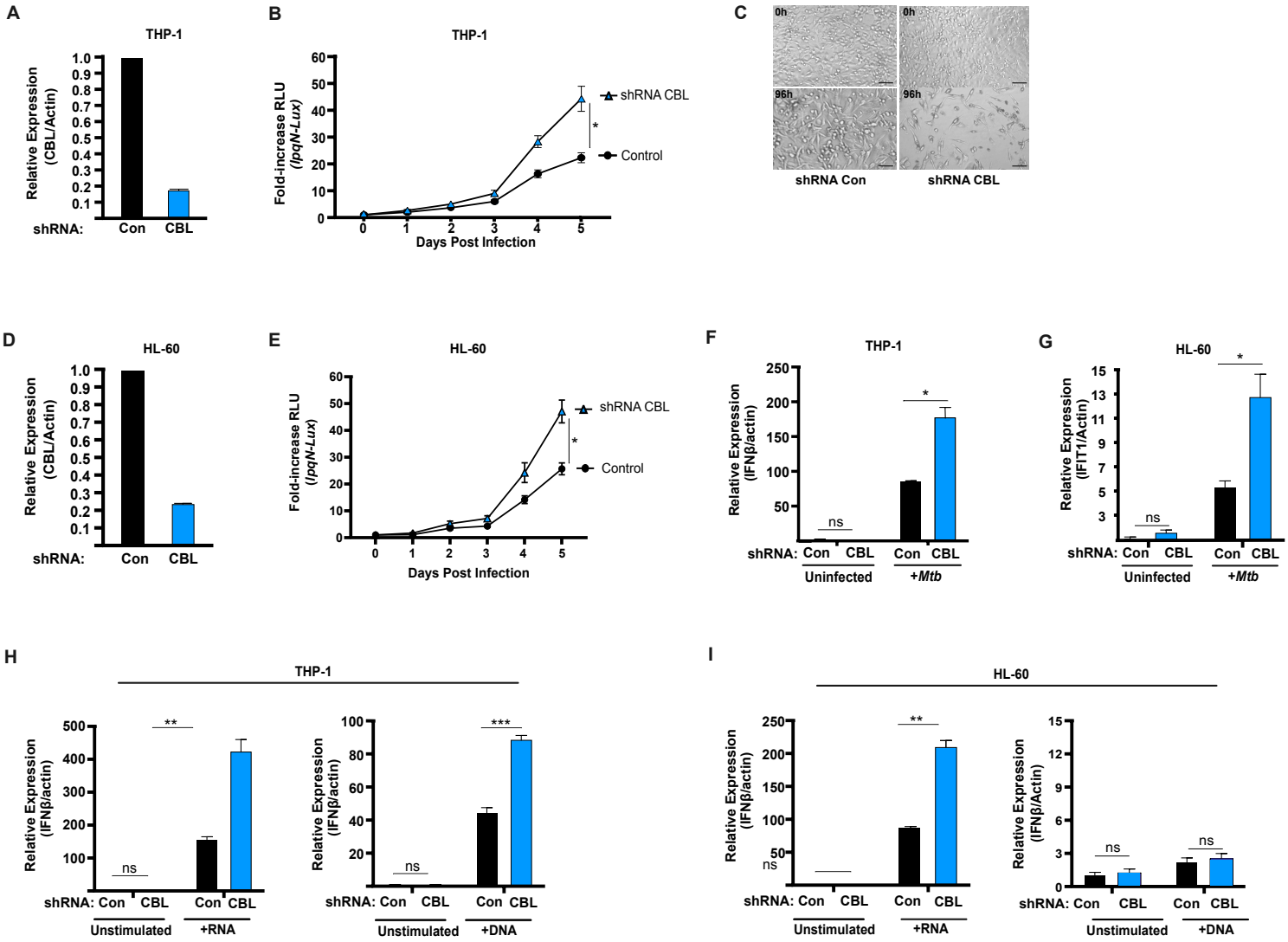
A
THP-1
Relative Expression (CBL/Actin)
shRNA: Con CBL
B
THP-1
Fold-increase RLU (lpqN-Lux)
Days Post Infection
shRNA CBL
Control
C
0h
96h
shRNA Con
shRNA CBL
D
HL-60
Relative Expression (CBL/Actin)
shRNA: Con CBL
E
HL-60
Fold-increase RLU (lpqN-Lux)
Days Post Infection
shRNA CBL
Control
F
THP-1
Relative Expression (IFNβ/actin)
shRNA: Con CBL Con CBL
Uninfected +Mtb
G
HL-60
Relative Expression (IFIT1/Actin)
shRNA: Con CBL Con CBL
Uninfected +Mtb
H
THP-1
Relative Expression (IFNβ/actin)
shRNA: Con CBL Con CBL
Unstimulated +RNA
Unstimulated +DNA
I
HL-60
Relative Expression (IFNβ/actin)
shRNA: Con CBL Con CBL
Unstimulated +RNA
Unstimulated +DNA

FIGURE 2

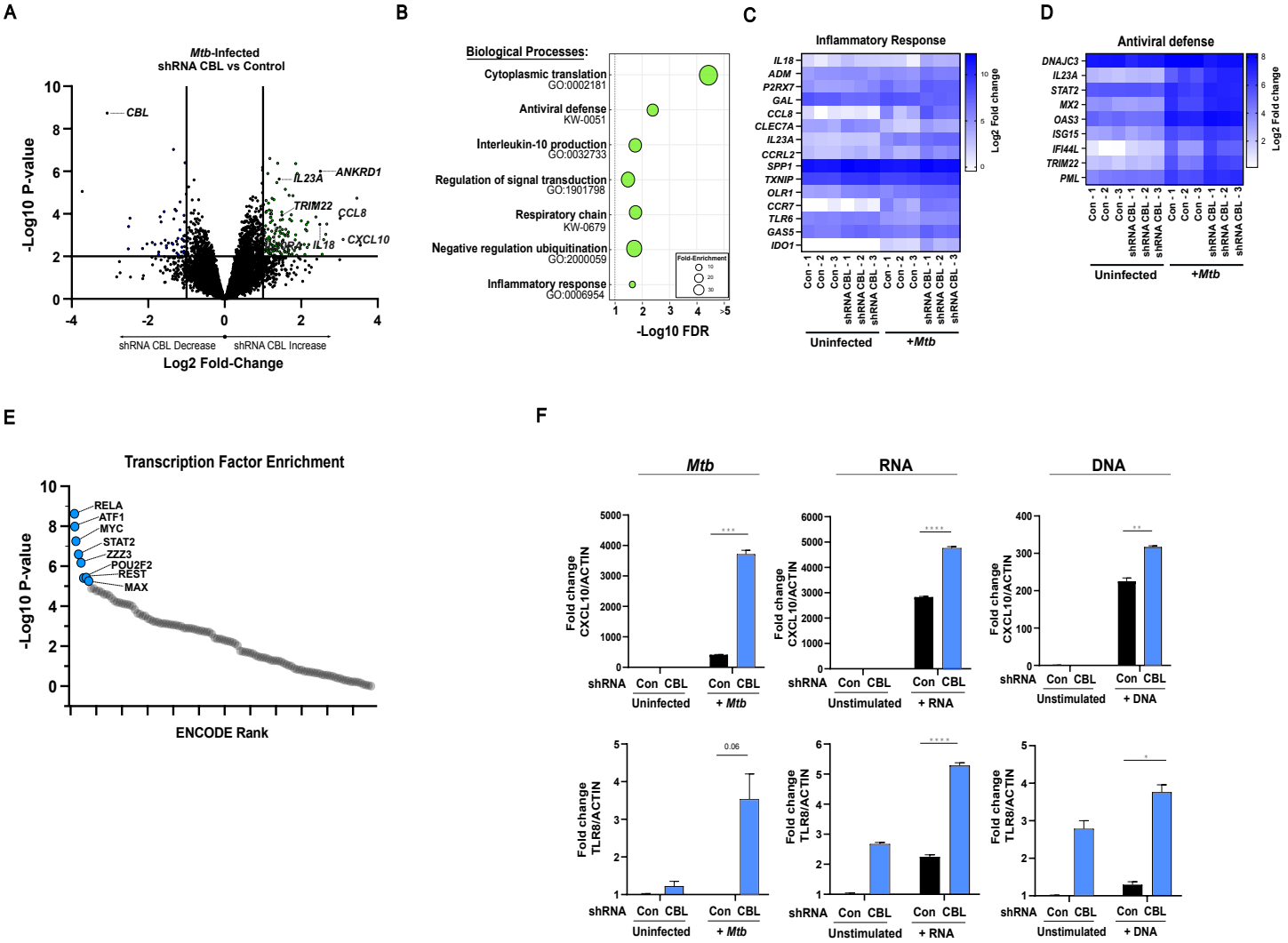
A
Mtb-Infected
shRNA CBL vs Control
-Log10 P-value
CBL
IL23A
ANKRD1
TRIM22
CCL8
IL18
CXCL10
shRNA CBL Decrease
shRNA CBL Increase
Log2 Fold-Change
B
Biological Processes:
Cytoplasmic translation
GO:0002181
Antiviral defense
KW-0051
Interleukin-10 production
GO:0032733
Regulation of signal transduction
GO:1901798
Respiratory chain
KW-0679
Negative regulation ubiquitination
GO:2000059
Inflammatory response
GO:0006954
Fold-Enrichment
-Log10 FDR
C
Inflammatory Response
IL18
ADM
P2RX7
GAL
CCL8
CLEC7A
IL23A
CCRL2
SPP1
TXNIP
OLR1
CCR7
TLR6
GAS5
IDO1
Log2 Fold change
Uninfected
+Mtb
D
Antiviral defense
DNAJC3
IL23A
STAT2
MX2
OAS3
ISG15
IFI44L
TRIM22
PML
Log2 Fold change
Uninfected
+Mtb
E
Transcription Factor Enrichment
-Log10 P-value
RELA
ATF1
MYC
STAT2
ZZZ3
POU2F2
REST
MAX
ENCODE Rank
F
Mtb
RNA
DNA
Fold change CXCL10/ACTIN
Fold change TLR8/ACTIN
shRNA
Con
CBL
Uninfected
+ Mtb
Unstimulated
+ RNA
+ DNA
0.06

FIGURE 3

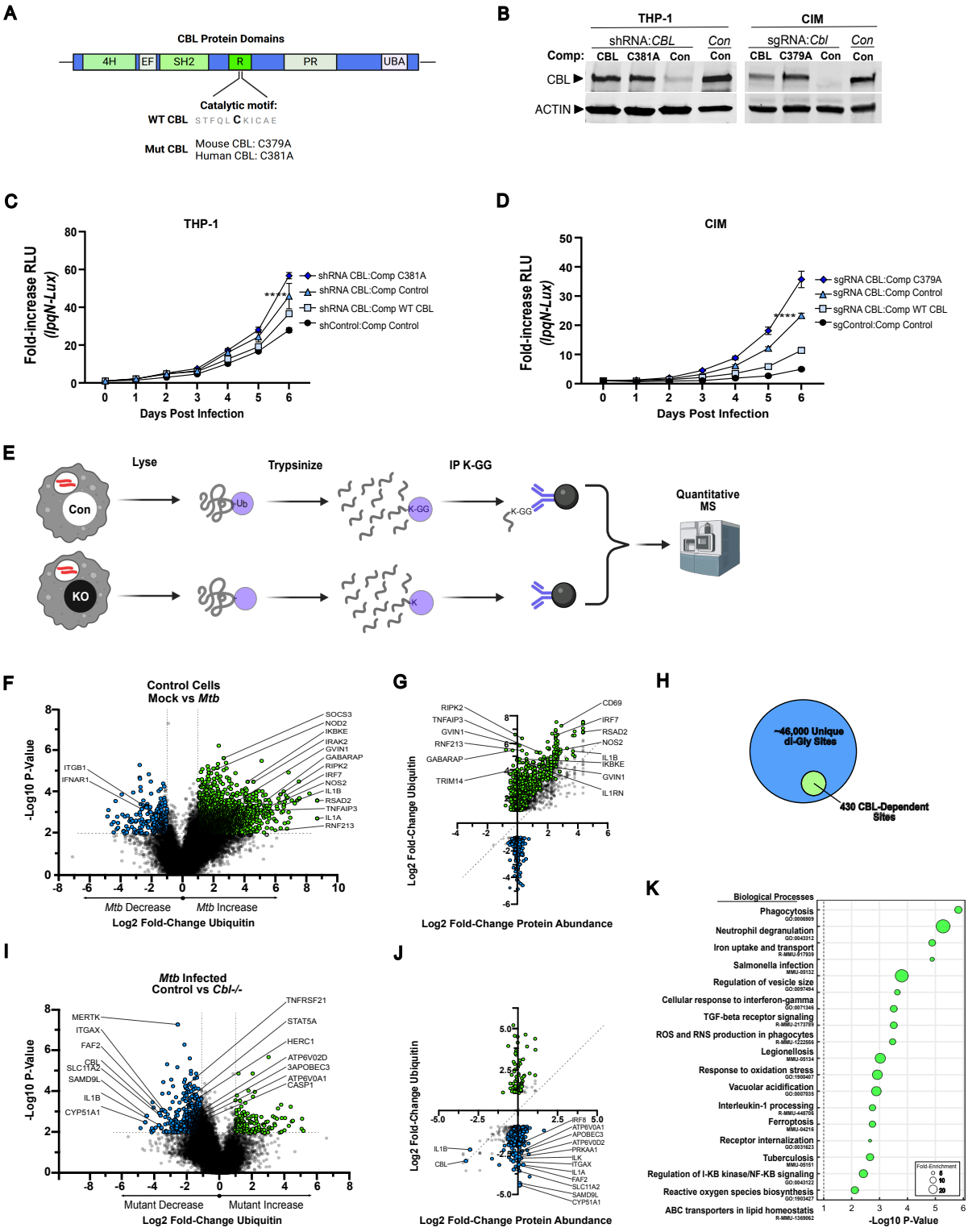
A
CBL Protein Domains
4H
EF
SH2
R
PR
UBA
Catalytic motif:
WT CBL STFQL C KICAE
Mut CBL Mouse CBL: C379A
Human CBL: C381A
B
THP-1
CIM
shRNA:CBL
Con
sgRNA:Cbl
Con
Comp: CBL C381A Con Con
CBL C379A Con Con
CBL
ACTIN
C
THP-1
Fold-increase RLU (lpqN-Lux)
Days Post Infection
shRNA CBL:Comp C381A
shRNA CBL:Comp Control
shRNA CBL:Comp WT CBL
shControl:Comp Control
D
CIM
Fold-increase RLU (lpqN-Lux)
Days Post Infection
sgRNA CBL:Comp C379A
sgRNA CBL:Comp Control
sgRNA CBL:Comp WT CBL
sgControl:Comp Control
E
Lyse
Trypsinize
IP K-GG
Quantitative MS
Con
KO
Ub
K-GG
K
F
Control Cells
Mock vs Mtb
-Log10 P-Value
Mtb Decrease
Mtb Increase
Log2 Fold-Change Ubiquitin
SOCS3
NOD2
IKBKE
IRAK2
GVIN1
GABARAP
RIPK2
IRF7
NOS2
IL1B
RSAD2
TNFAIP3
IL1A
RNF213
ITGB1
IFNAR1
G
Log2 Fold-Change Ubiquitin
Log2 Fold-Change Protein Abundance
RIPK2
TNFAIP3
GVIN1
RNF213
GABARAP
TRIM14
CD69
IRF7
RSAD2
NOS2
IL1B
IKBKE
GVIN1
IL1RN
H
~46,000 Unique di-Gly Sites
430 CBL-Dependent Sites
I
Mtb Infected
Control vs Cbl-/-
-Log10 P-Value
Mutant Decrease
Mutant Increase
Log2 Fold-Change Ubiquitin
MERTK
ITGAX
FAF2
CBL
SLC11A2
SAMD9L
IL1B
CYP51A1
TNFRSF21
STAT5A
HERC1
ATP6V02D
3APOBEC3
ATP6V0A1
CASP1
J
Log2 Fold-Change Ubiquitin
Log2 Fold-Change Protein Abundance
IRF8
ATP6V0A1
APOBEC3
ATP6V0D2
PRKAA1
ILK
ITGAX
IL1A
FAF2
SLC11A2
SAMD9L
CYP51A1
IL1B
CBL
K
Biological Processes
Phagocytosis
Neutrophil degranulation
Iron uptake and transport
Salmonella infection
Regulation of vesicle size
Cellular response to interferon-gamma
TGF-beta receptor signaling
ROS and RNS production in phagocytes
Legionellosis
Response to oxidation stress
Vacuolar acidification
Interleukin-1 processing
Ferroptosis
Receptor internalization
Tuberculosis
Regulation of I-KB kinase/NF-KB signaling
Reactive oxygen species biosynthesis
ABC transporters in lipid homeostatis
Fold-Enrichment
-Log10 P-Value

FIGURE 4

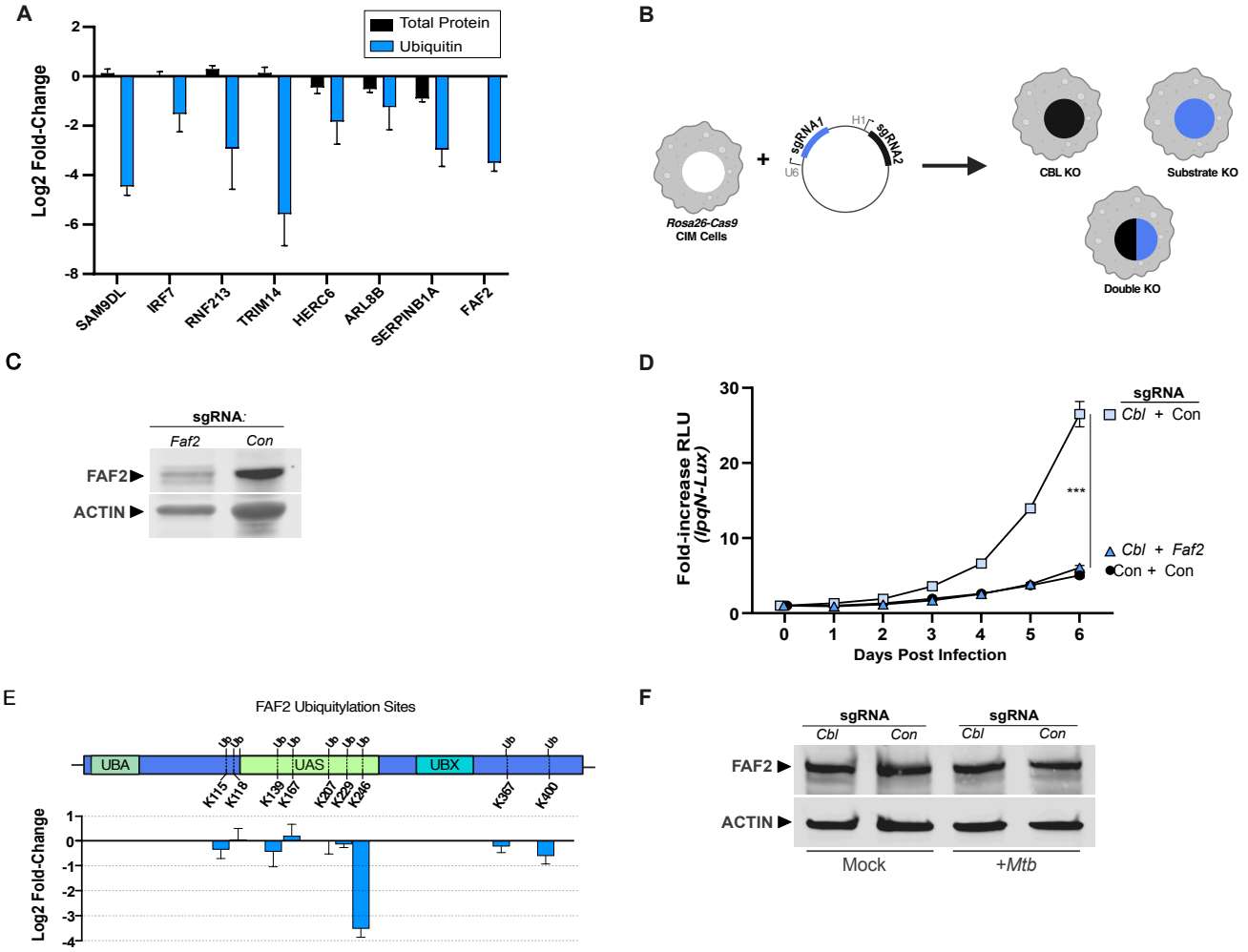
A
Total Protein
Ubiquitin
Log2 Fold-Change
2
0
-2
-4
-6
-8
SAM9DL
IRF7
RNF213
TRIM14
HERC6
ARL8B
SERPINB1A
FAF2
B
Rosa26-Cas9
CIM Cells
sgRNA1
sgRNA2
H1
U6
CBL KO
Substrate KO
Double KO
C
sgRNA:
Faf2
Con
FAF2
ACTIN
D
Fold-increase RLU
(lpqN-Lux)
30
20
10
0
sgRNA
Cbl + Con
Cbl + Faf2
Con + Con
***
0
1
2
3
4
5
6
Days Post Infection
E
FAF2 Ubiquitylation Sites
UBA
UAS
UBX
Ub
K115
K118
K139
K167
K207
K229
K246
K367
K400
Log2 Fold-Change
1
0
-1
-2
-3
-4
F
sgRNA
Cbl
Con
Cbl
Con
FAF2
ACTIN
Mock
+Mtb